Bibliography

[1] R. Ansola, J. Canales, J.A. Tarrago, and J. Rasmussen. On simultaneous shape and material layout optimization of shell structures. *Struct. Multidisc. Optim.*, 24:175–184, 2002.

[2] R. Ansola, J. Canales, J.A. Tarrago, and J. Rasmussen. Combined shape and reinforcement layout optimization of shell structures. *Struct. Multidisc. Optim.*, 27:219–227, 2004.

[3] G.I.N. Rozvany, editor. *Topology Optimization in Structural Mechanics*. Springer-Verlag, Wien, New York, 1997.

[4] M.P. Bendsøe and O. Sigmund. *Topology Optimization: Theory, Methods and Applications*. Springer, Berlin, 2003.

[5] P. Duysinx and O. Sigmund. New developments in handling stress constraints in optimal material distributions. In *Proceedings of the 7th AIAA/USAF/NASA/ISSMO symposium on Multidisciplinary Design Optimization*, Saint Louis, Missouri, USA, September 1998.

[6] P. Duysinx and M.P. Bendsøe. Topology optimization of continuum structures with local stress constraints. *Int. J. Numer. Meth. Engng.*, 43:1453–1478, 1998.

[7] G.I.N. Rozvany. On design-dependent constraints and singular topologies. *Struct. Multidisc. Optim.*, 21:164 – 172, 2001.

[8] R.T. Haftka, Z. Gürdal, and M.P. Kamat. *Elements of structural optimization*. Kluwer Academic, Dordrecht, 2nd edition, 1990.

[9] J.A. Snyman. *Practical Mathematical Optimization: An introduction to the basic optimization theory and classical and new gradient-based algorithms*. Springer Science+Business Media, Inc., 233 Spring Street, New York, NY, 10013, USA, 2005.

[10] K. Svanberg. The method of moving asymptotes - a new method for structural optimization. *Int. J. Numer. Meth. Engng.*, 24:359–373, 1987.

[11] C. Niezrecki, D. Brei, S. Balakrishnan, and A. Moskalik. Piezoelectric actuation: State of the art. *The Shock and Vibration Digest*, 33:269–280, 2001.

[12] S.E. Park and T.R. Shrout. Ultrahigh strain and piezoelectric behavior in relaxor based ferroelectric single crystals. *Journal of Applied Physics*, 82:1804–1811, 1997.

[13] O. Sigmund and J. Petersson. Numerical instabilities in topology optimization: A survey on procedures dealing with checkerboards, mesh-dependencies and local minima. *Struct. Multidisc. Optim.*, 16:68 – 75, 1998.

[14] A. Díaz and O. Sigmund. Checkerboard patterns in layout optimization. *Struct. Optim.*, 10:40–45, 1995.

[15] T.A. Poulsen. A simple scheme to prevent checkerboard patterns and one-node connected hinges in topology optimization. *Struct. Multidisc. Optim.*, 24:396–399, 2002.

[16] K.-J. Bathe. *Finite Element Procedures*. Prentice-Hall International, Inc., Upper Saddle River, New Jersey 07458, 1996.

[17] R.D. Cook, D.S. Malkus, Plesha M.E., and R.J. Witt. *Concepts and applications of finite element analysis*. John Wiley and Sons, New York, 2002.

[18] T.J.R. Hughes and F. Brezzi. On drilling degrees of freedom. *Comput. Methods Appl. Mech. Engrg.*, 72:105–121, 1989.

[19] C.A. Felippa. A historical outline of matrix structural analysis: a play in three acts. *Computers and Structures*, 79:1313–1324, 2001.

[20] G. Pimpinelli. An assumed strain quadrilateral element with drilling degrees of freedom. *Finite Elements in Analysis and Design*, 41:267–283, 2004.

[21] A. Ibrahimbegovic, R.L. Taylor, and E.L. Wilson. A robust quadrilateral membrane finite element with drilling degrees of freedom. *Int. J. Numer. Meth. Engng.*, 30:445–457, 1990.

[22] O.C. Zienkiewicz and R.L. Taylor. *The Finite Element Method*, volume II: Solid and Fluid Mechanics Dynamics and Non-linearity. McGraw-Hill Book Company, London, 1991.

[23] D.J. Allman. A quadrilateral finite element including vertex rotations for plane elasticity analysis. *Int. J. Numer. Meth. Engng.*, 26:717–730, 1988.

[24] R.H. MacNeal and R.L. Harder. A refined four-noded membrane element with rotational degrees of freedom. *Computers and Structures*, 28:75–84, 1988.

[25] F. Frey. Shell finite elements with six degrees of freedom per node. In *ASME Winter Annual Meeting*, San Francisco, 1989.

[26] P.G. Bergan and C.A. Felippa. A triangular membrane element with rotational degrees of freedom. *Comput. Methods Appl. Mech. Engrg.*, 50:25–69, 1985.

[27] A.A. Groenwold. Finite element analysis of composite plates and shells. Master's thesis, University of Pretoria, Dept. of Mechanical and Aeronautical Engineering, Pretoria, South Africa, 1993.

[28] L. Jin. Analysis and evaluation of a shell finite element with drilling degrees of freedom. Master's thesis, University of Maryland at College Park, Dept. of Civil Engineering and Institute for System Research, 1994.

[29] A.C. Scordelis. Analysis of continuum box girder bridges. Technical Report SESM 67-2, University of California, Dept. of Civil Engineering, Berkley, CA, 1967.

[30] K.J. Willam. *Finite element analysis of cellular structures*. PhD thesis, University of California, Dept. of Civil Engineering, Berkley, CA, 1969.

[31] B. Irons and S. Ahmad. *Techniques of finite elements*. Ellis-Horwood, Cichester, U.K., 1980.

[32] D.J. Allman. A compatible triangular element including vertex rotations for plane elasticity analysis. *Computers and Structures*, 19:1–8, 1984.

[33] R.D. Cook. On the allman triangle and a related quadrilateral elements. *Computers and Structures*, 22:1065–1067, 1986.

[34] P. Jetteur. A shallow shell element with in-plane rotational degrees of freedom. IREM Internal Report 86/3, Ecole Polytechnique Fédérale de Lausanne, 1986.

[35] P. Jetteur. Improvement of the quadrilateral "JET" shell element for a particular class of shell problems. IREM Internal Report 87/1, Ecole Polytechnique Fédérale de Lausanne, 1987.

[36] S. Jaamei. "Jet" thin shell finite element with drilling rotations. IREM Internal Report 88/7, Ecole Polytechnique Fédérale de Lausanne, 1988.

[37] R.L. Taylor and J.C. Simo. Bending and membrane elements for analysis of thick and thin shells. In G.N. Pande and J. Middleton, editors, *Proceedings of the NUMETA 85 Conference*, Swansea, 7-11 Jan. 1985.

[38] R.L. Taylor. Finite element analysis of linear shell problems. In J.R. Whiteman, editor, *The Mathematics of Finite Elements and Applications VI, MAFELAP*, pages 191–203, Academic Press Limited, London, 1987.

[39] J.C. Simo, D.D. Fox, and M.S. Rifai. On a stress resultant geometrically exact shell model Part II: The linear theory; computational aspects. *Comput. Methods Appl. Mech. Engrg.*, 73:53–92, 1989.

[40] E. Reissner. A note on variational principles in elasticity. *International Journal of Solids and Structures*, 1:93–95, 1965.

[41] T.J.R. Hughes, F. Brezzi, A. Masud, and I. Harari. Finite element with drilling degree of freedom: Theory and numerical evaluation. In R. Gruber, J. Periaux, and R.P. Shaw, editors, *Proceedings of the fifth International Symposium on Numerical Methods in Engineering*, volume 1, pages 3–17, Springer-Verlag, Berlin, 1989.

[42] A. Ibrahimbegovic and E.L. Wilson. A unified formulation for triangular and quadrilateral flat shell finite elements with six nodal degrees of freedom. *Communications in Applied Numerical Methods*, 7:1–9, 1991.

[43] S. Geyer and A.A. Groenwold. Two hybrid stress membrane finite element families with drilling rotations. *Int. J. Numer. Meth. Engng.*, 53:583–601, 2002.

[44] T.J.R. Hughes, A. Masud, and I. Harari. Numerical assessment of some membrane elements with drilling degrees of freedom. *Computers and Structures*, 55:297–314, 1995.

[45] S. Geyer and A.A. Groenwold. On reduced integration and locking of flat shell finite elements with drilling rotations. *Commun. Num. Meth. Eng.*, 19:85–97, 2003.

[46] T.H.H. Pian. Derivation of element stiffness matrices by assumed stress distributions. *AIAA J.*, 2:1333–1336, 1964.

[47] T.H.H. Pian. State-of-the-art development of the hybrid/mixed finite element method. *Fin. Elem. Anal. Des.*, 21:5–20, 1995.

[48] M.A. Aminpour. An assumed-stress hybrid 4-node shell element with drilling degrees of freedom. *Int. J. Numer. Meth. Engng.*, 33:19–38, 1992.

[49] G. Rengarajan, M.A. Aminpour, and N.F. Knight. Improved assumed-stress hybrid shell element with drilling degrees of freedom for linear stress, buckling and free vibration analyses. *Int. J. Numer. Meth. Engng.*, 38:1917–1943, 1995.

[50] K.Y. Sze and A. Ghali. Hybrid plane quadrilateral element with corner rotations. *ASCE Journal of Structural Engineering*, 119:2552–2572, 1993.

[51] K.Y. Sze, C. Wanji, and Y.K. Cheung. An efficient quadrilateral plane element with drilling degrees of freedom using orthogonal stress modes. *Computers and Structures*, 42:695–705, 1992.

[52] A.A. Groenwold and N. Stander. An efficient 4-node 24 d.o.f. thick shell finite element with 5-point quadrature. *Engineering Computations*, 12:723–748, 1995.

[53] A.A. Groenwold and N. Stander. A 24 d.o.f. 4-node flat shell finite element for general unsymmetric orthotropic layered composites. *Engineering Computations*, 15:518–543, 1998.

[54] H.H. Dovey. *Extension of three dimensional analysis to shell structures using the finite element idealization.* Report no. UC SESM 74-2, Ph-D dissertation, University of California, Berkeley, 1974.

[55] C.A. Felippa. *Advanced Finite Element Methods (ASEN 5367): Course Material*. Aerospace Engineering Sciences - University of Colorado at Boulder, 2006. Available at http://www.colorado.edu/engineering/CAS/courses.d/AFEM.d/Home.html.

[56] T. Mura and T. Koya. *Variational Methods in Mechanics*. Oxford University Press, Inc., 200 Madison Avenue, New York, New York, 10016, 1992.

[57] T.J.R. Hughes. *The finite element method: Linear static and dynamic analysis*. Prentice-Hall, London, 1987.

[58] C.S. Long, S. Geyer, and A.A. Groenwold. A numerical study of the effect of penalty parameters for membrane elements with independent rotation fields and penalized equilibrium. *Finite Elements in Analysis and Design*, 42:757–765, 2006.

[59] J.C. Simo and M.S. Rifai. A class of mixed assumed strain methods and the method of incompatible modes. *Int. J. Numer. Meth. Engng.*, 29:1595–1638, 1990.

[60] O.C. Zienkiewicz and R.L. Taylor. *The Finite Element Method*, volume I: Basic Formulation and Linear Problems. McGraw-Hill Book Company, London, 1989.

[61] S. Di and E. Ramm. On alternative hybrid stress 2D and 3D elements. *Engineering Computations*, 11:49–68, 1994.

[62] T.H.H. Pian and K. Sumihara. Rational approach for assumed stress finite elements. *Int. J. Numer. Meth. Engng.*, 20:1685–1695, 1984.

[63] A.A. Groenwold, Q.Z. Xiao, and N.J. Theron. Accurate solution of traction free boundaries using hybrid stress membrane elements with drilling degrees of freedom. *Comput. Struct.*, 82:2071–2081, 2004.

[64] K.Y. Sze, X.-M. Yang, and L.-Q. Yao. Stabilized plane and axisymmetric piezoelectric finite element models. *Finite Elements in Analysis and Design*, 40:1105–1122, 2004.

[65] C.C. Wu, K.Y. Sze, and Y.Q. Huang. Numerical solutions on fracture of piezoelectric materials by hybrid element. *International Journal of Solids and Structures*, 38:4315–4329, 2001.

[66] A.A. Cannarozzi and F. Ubertini. Some hybrid variational methods for linear electroelasticity problems. *International Journal of Solids and Structures*, 38:2573–2596, 2001.

[67] P. Heyliger. A note on the static behaviour of simply-supported laminated piezoelectric cylinders. *International Journal of Solids and Structures*, 34:3781–3794, 1997.

[68] S. Kapuria, S. Sengupta, and P.C. Dumir. Three-dimensional solution for simply-supported piezoelectric cylindrical shell for axisymmetric load. *Comput. Methods Appl. Mech. Engrg.*, 140:139–155, 1997.

[69] H. Allik and T.J.R. Hughes. Finite element method for piezoelectric vibration. *Int. J. Numer. Meth. Engng.*, 2:151–157, 1970.

[70] A. Benjeddou. Advances in piezoelectric finite element modeling of adaptive structural elements: a survey. *Computers and Structures*, 76:347–363, 2000.

[71] J.S. Yang. Mixed variational principles for piezoelectric elasticity. In B. Antar, R. Engels, A.A. Prinaris, T.H. Moulden, and O. Zanaboni, editors, *Developments in Theoretical and Applied Mechanics*, volume XVI, pages II.1.31–38, University of Tennessee Space Institute, Tennessee, 1992.

[72] E.P. EerNisse. Variational method for electroelastic vibration analysis. *IEEE Transactions on Sonics and Ultrasonics*, SU-14:153–160, 1967.

[73] R. Holland and E.P. EerNisse. Variational evaluation of admittances of multielectroded three-dimensional piezoelectric structures. *IEEE Transactions on Sonics and Ultrasonics*, SU-15:119–132, 1968.

[74] K.Y. Sze, L.Q. Yao, and S. Yi. A hybrid stress ANS solid-shell element and its generalization for smart structure modelling. Part II - smart structure modelling. *Int. J. Numer. Meth. Engng.*, 48:565–582, 2000.

[75] K.Y. Sze and L.Q. Yao. Modelling smart structures with segmented piezoelectric sensors and actuators. *Journal of Sound and Vibration*, 235:495–520, 2000.

[76] K.Y. Sze and Y.S. Pan. Hybrid finite element models for piezoelectric materials. *Journal of Sound and Vibration*, 226:519–547, 1999.

[77] C.S. Long, P.W. Loveday, and A.A. Groenwold. Design of a piezoelectric mirror scanning device using topology optimization. In *Proc. Sixth World Congress on Structural and Multidisciplinary Optimization*, Rio de Janeiro, Brazil, May 2005. Paper no. 4031.

[78] T. Ikeda. *Fundamentals of Piezoelectricity*. Oxford University Press, Oxford, 1996.

[79] M. Liu. Finite element analysis for cracked piezoelectric material. Master's thesis, Dept. of Modern Mechanics, Univ. of Sci. and Tech. of China, Hefei, 1998.

[80] C.S. Long, P.W. Loveday, and A.A. Groenwold. Planar four node piezoelectric elements with drilling degrees of freedom. *Int. J. Numer. Meth. Engng.*, 65:1802–1830, 2006.

[81] T.J.R. Hughes, A. Masud, and I. Harari. Numerical assessment of some membrane elements with drilling degrees of freedom. *Computers and Structures*, 55:297–314, 1995.

[82] T.J.R. Hughes, A. Masud, and I. Harari. Dynamic analysis and drilling degrees of freedom. *Int. J. Numer. Meth. Engng.*, 38:3193–3210, 1995.

[83] H.S. Tzou. *Piezoelectric Shells: Distributed Sensing and Control of Continua*. Kluwer Academic Publishers, Netherlands, 1993.

[84] V.M. Franco Correia, M.A. Aguiar Gomes, A. Suleman, C.M. Mota Soares, and C.A. Mota Soares. Modelling and design of adaptive composite structures. *Comput. Methods Appl. Mech. Engrg.*, 185:325–346, 2000.

[85] R.H. MacNeal and R.L. Harder. A proposed standard set of problems to test finite element accuracy. *Finite Elements in Analysis and Design*, 1:3–20, 1985.

[86] O.C. Zienkiewicz, R.L. Taylor, and J.M. Too. Reduced integration techniques in general analysis of plates and shells. *Int. J. Numer. Meth. Engng.*, 3:275–290, 1971.

[87] B.M. Irons. Quadrature rules for brick based finite elements. *Int. J. Numer. Meth. Engng.*, 3:293–294, 1971.

[88] A.K. Gupta and B. Mohraz. A method of computing numerically integrated stiffness matrices. *Int. J. Numer. Meth. Engng.*, 5:83–89, 1972.

[89] T. Belytschko and B.E. Engelman. On flexurally superconvergent four-node quadrilaterals. *Computers and Structures*, 25:909–918, 1987.

[90] T. Belytschko, C.S. Tsay, and W.K. Liu. A stabilization matrix for the bilinear Mindlin plate element. *Comp. Meth. Applied Mech. Eng.*, 29:313–327, 1981.

[91] T. Belytschko and C.S. Tsay. A stabilization procedure for the quadrilateral plate with one-point quadrature. *Int. J. Numer. Meth. Engng.*, 19:405–419, 1983.

[92] X.J. Wang and T. Belytschko. A study of stabilization and projection in the 4-node Mindlin plate element. *Int. J. Numer. Meth. Engng.*, 28:2223–2238, 1989.

[93] W.K. Liu, J.S-J Ong, and Uras R.A. Finite element stabilization matrices - A unification approach. *Comp. Meth. Applied Mech. Eng.*, 53:13–46, 1985.

[94] T.J.R. Hughes, M. Cohen, and M. Haroun. Reduced and selective integration techniques in the finite element analysis of plates. *Nucl. Eng. Design*, 46:203–222, 1978.

[95] N. Stander and E.L. Wilson. A 4-node quadrilateral membrane element with in-plane vertex rotations and modified reduced quadrature. *Engineering Computations*, 6:266–271, 1989.

[96] K.-J Bathe and E.N. Dvorkin. A formulation of general shell elements - The use of mixed interpolation of tensorial components. *Int. J. Numer. Meth. Engng.*, 22:697–722, 1986.

[97] N. Bićanić and E. Hinton. Spurious modes in two-dimensional isoparametric elements. *Int. J. Numer. Meth. Engng.*, 14:1545–1557, 1979.

[98] T.A. Poulsen. Topology optimization in wavelet space. *Int. J. Numer. Meth. Engng.*, 53:567–582, 2002.

[99] G.I.N. Rozvany, V. Pomezanski, Z. Gaspar, and O.M. Querin. Some pivotal issues in structural topology optimization. In *Proceeding of the 6th World Congress on Structural and Multidisciplinary Optimization*, Rio de Janeiro, Brazil, May 2005. Paper no. 5951.

[100] O. Sigmund. On the design of compliant mechanisms using topology optimization. *Mechanics of Structures and Machines*, 25:495–526, 1997.

[101] O. Sigmund. A 99 line topology optimization code written in Matlab. *Struct. Multidisc. Optim.*, 21:120–127, 2001.

[102] C.S. Jog and R.B. Haber. Stability of finite element models for distributed-parameter optimization and topology design. *Comput. Methods Appl. Mech. Engrg.*, 130:203–226, 1996.

[103] M.I. Frecker. Review of current research activities in optimization of smart structures and actuators. In V. S. Rao, editor, *Proc. SPIE Vol. 4693, p. 112-123, Smart Structures and Materials 2002: Modeling, Signal Processing, and Control, Vittal S. Rao; Ed.*, pages 112–123, Jul 2002.

[104] N.L. Pedersen. Maximization of eigenvalues using topology optimization. *Struct. Multidisc. Optim.*, 20:2–11, 2000.

[105] A.P. Seyranian, E. Lund, and N. Olhoff. Multiple eigenvalues in structural optimization problems. *Struct. Optim.*, 8:207–227, 1994.

[106] O. Sigmund. Design of multiphysics actuators using topology optimization - Part II: Two-material structures. *Comput. Methods Appl. Mech. Engrg.*, 190:6605–6627, 2001.

[107] M.P. Bendsøe and N. Kikuchi. Generating optimal topologies in structural design using a homogenization method. *Comput. Methods Appl. Mech. Engrg.*, 71:197–224, 1988.

[108] K.-T. Cheng and N. Olhoff. An investigation concerning optimal design of solid elastic plates. *International Journal of Solids and Structures*, 17:305–323, 1981.

[109] M.P. Bendsøe. Optimal shape design as a material distribution problem. *Struct. Optim.*, 1:193–202, 1989.

[110] M. Zhou and G.I.N. Rozvany. The COC algorithm, Part II: Topological, geometrical and generalized shape optimization. *Comp. Meth. Appl. Mech. Engng.*, 89:309–336, 1991.

[111] G.I.N. Rozvany, M. Zhou, and T. Birker. Generalized shape optimization without homogenization. *Struct. Optim.*, 4:250–252, 1992.

[112] L.H. Tenek and I. Hagiwara. Optimization of material distribution within isotropic and anisotropic plates using homogenization. *Comput. Methods Appl. Mech. Engrg.*, 109:155–167, 1992.

[113] L.H. Tenek and I. Hagiwara. Optimal rectangular plate and shallow shell topologies using thickness distribution or homogenization. *Comput. Methods Appl. Mech. Engrg.*, 115:111–124, 1994.

[114] A.R. Díaz, R. Lipton, and C.A. Soto. A new formulation of the problem of optimum reinforcement of reissner-mindlin plates. *Comput. Methods Appl. Mech. Engrg.*, 123:121–139, 1995.

[115] L.A. Krog and N. Olhoff. Optimum topology and reinforcement design of disk and plate structures with multiple stiffness and eigenfrequency objectives. *Computers and Structures*, 72:535–563, 1999.

[116] S.J. Lee, J.E. Bae, and E. Hinton. Shell topology optimization using layered artificial material model. *Int. J. Numer. Meth. Engng.*, 47:843–867, 2000.

[117] F. Belblidia, J.E.B. Lee, S. Rechak, and E. Hinton. Topology optimization of plate structures using single- or three-layered artificial material model. *Advances in Engineering Software*, 32:159–168, 2001.

[118] W. Kanok-Nukulchai. A simple and efficient finite element for general shell analysis. *Int. J. Numer. Meth. Engng.*, 14:179–200, 1979.

[119] N.L. Pedersen. Topology optimization of laminated plates with prestress. *Computers and Structures*, 80:559–570, 2002.

[120] C.S. Jog. Topology design of structures subjected to periodic loading. *Journal of Sound and Vibration*, 253:687–709, 2002.

[121] J. Stegmann and E. Lund. Nonlinear topology optimization of layered shell structures. *Struct. Multidisc. Optim.*, 29:349 – 360, 2005.

[122] F. Belblidia and S. Bulman. Constrained adaptive topology optimization for vibrating shell structures. *Struct. Multidisc. Optim.*, 22:167–176, 2001.

[123] S. Bulman, J. Sienz, and E. Hinton. Comparisons between algorithms for structural topology optimization using a series of benchmark studies. *Computers and Structures*, 79:1203–1218, 2001.

[124] F. Belblidia and S. Bulman. A hybrid topology optimization algorithm for static and vibrating shell structures. *Int. J. Numer. Meth. Engng.*, 54:835–852, 2002.

[125] J.-L. Batoz and M. Ben Tahar. Evaluation of a new quadrilateral thin plate bending element. *Int. J. Numer. Meth. Engng.*, 18:1655–1677, 1982.

[126] K.-J. Bathe and E.N. Dvorkin. A four-node plate bending element based on Mindlin/Reissner plate theory and a mixed interpolation. *Int. J. Numer. Meth. Engng.*, 21:367–383, 1985.

[127] E. Dvorkin and K.-J. Bathe. A continuum mechanics based four node shell element for general nonlinear analysis. *Engineering Computations*, 1:77–88, 1984.

[128] R.H. MacNeal. Derivation of element stiffness matrices by assumed strain distribution. *Nuclear Engineering Design*, 70:3–12, 1982.

[129] T.J.R. Hughes and T.E. Tezduyar. Finite elements based upon mindlin plate theory, with particular reference to the 4-node bilinear isoparametric element. *Journal of Applied Mechanics*, 48:587–595, 1981.

[130] S.J. Lee and E. Hinton. Dangers inherited in shells optimized with linear assumptions. *Computers and Structures*, 78:473–486, 2000.

[131] M. Kögl and E.C.N. Silva. Topology optimization of smart structures: design of piezoelectric plate and shell actuators. *Smart Mater. Struct.*, 14:387–399, 2005.

[132] J. Stegmann and E. Lund. Discrete material optimization of general composite shell structures. *Int. J. Numer. Meth. Engng.*, 62:2009–2027, 2005.

[133] M.K. Rao and U. Shrinivasa. A set of pathological tests to validate new finite elements. *Sadhana*, 26:549–590, 2001.

[134] J. Stegmann and E. Lund. Nonlinear topology optimization of layered shell structures. *Struct. Multidisc. Optim.*, 29:349–360, 2005.

[135] C.S. Long, A.A. Groenwold, and P.W. Loveday. Implications of finite element formulation in optimal topology design. In A. Zingoni, editor, *Progress in Structural Engineering, Mechanics and Computation*, pages 1015–1019, Cape Town, South Africa, July 2004.

[136] A.R. Díaz and N. Kikuchi. Solutions to shape and topology eigenvalue optimization problems using a homogenization method. *Int. J. Numer. Meth. Engng.*, 35:1487–1502, 1992.

[137] T.E. Bruns and Tortorelli D.A. Topology optimization of non-linear elastic structures and compliant mechanisms. *Comput. Methods Appl. Mech. Engrg.*, 190:3443–3459, 2001.

[138] O. Sigmund. Design of multiphysics actuators using topology optimization - Part I: One-material structures. *Comput. Methods Appl. Mech. Engrg.*, 190:6577–6604, 2001.

[139] M.P. Bendsøe. *Optimization of structural topology, shape, and material*. Springer, Berlin, 1995.

[140] C.S. Long and A.A. Groenwold. Reduced modified quadrature for quadratic membrane finite elements. *Int. J. Num. Meth. Eng.*, 61:837–855, 2004.

[141] Hassani B.; Hinton E. A review of homogenization and topology opimization II-analytical and numerical solution of homogenization equations. *Computers and Structures*, 69:719–738, 1998.

[142] Hassani B.; Hinton E. A review of homogenization and topology optimization I-homogenization theory for media with periodic structure. *Computers and Structures*, 69:707–717, 1998.

[143] Hassani B.; Hinton E. A review of homogenization and topology optimization III-topology optimization using optimality criteria. *Computers and Structures*, 69:739–756, 1998.

[144] O. Sigmund. Materials with prescribed constitutive parameters: an inverse homogenization problem. *International Journal of Solids and Structures*, 31:2313–2329, 1994.

[145] C.S. Jog, R.B. Haber, and M.P. Bendsøe. A displacement-based topology design method with self-adaptive layered materials. In M.P. Bendsøe and C.A. Mota Soares, editors, *Topology Design of Structures*, Dordrecht, The Netherlands, 1993. Kluwer Academic Publishers.

[146] C.S. Long, P.W. Loveday, and A.A. Groenwold. On membrane elements with drilling degrees of freedom in topology optimization. In *Proc. Fifth World Congress on Structural and Multidisciplinary Optimization*, Lido di Jesolo, Venice, Italy, May 2003. Paper no. 83.

[147] C.S. Long, P.W. Loveday, and A.A. Groenwold. Topology optimization of generally curved shells. *Finite Elements in Analysis and Design*, 2006. To be submitted.

[148] C.-K. Choi, K.-Y. Chung, and E.-J. Lee. Mixed formulated 13-node hexahedral elements with rotational degrees of freedom: MR-H13 elements. *Structural Engineering and Mechanics*, 11:105–122, 2001.

[149] H.A. Eschenauer and N. Olhoff. Topology optimization of continuum structures: A review. *Applied Mechanics Reviews*, 54:331–390, 2001.

[150] T.E. Bruns. A reevaluation of the simp method with filtering and an alternative formulation for solid-void topology optimization. *Struct. Multidisc. Optim.*, 30:428–436, 2005.

[151] Y.Y. Kim and G.H. Yoon. Multi-resolution multi-scale topology optimization - a new paradigm. *International Journal of Solids and Structures*, 37:5529–5559, 2000.

[152] M.P. Bendsøe and O. Sigmund. Material interpolation schemes in topology optimization. *Archives of Applied Mechanics*, 69:635–654, 1999.

[153] S. Min, N. Kikuchi, Y.C. Park, S. Kim, and S. Chang. Optimal topology design of structures under dynamic loads. *Struct. Optim.*, 17:208–218, 1999.

[154] S. Min, S. Nishiwaki, and N. Kikuchi. Unified topology design of static and vibrating structures using multiobjective optimization. *Computers and Structures*, 75:93–116, 2000.

[155] S.J. Min and N. Kikuchi. Optimal reinforcement design of structures under the buckling load using the homogenization design method. *Structural Engineering and Mechanics*, 5:565–576, 1997.

[156] T. Borrvall and J. Petersson. Topology optimization of fluids in Stokes flow. *International Journal for Numerical Methods in Fluids*, 41:77–107, 2003.

[157] J.S. Jensen and O. Sigmund. Topology optimization of two-dimensional waveguides. In *Short papers of the 5th World Congress on Structural and Multidisciplinary Optimization WCSMO5*, pages 125–126, Lido de Jesolo, Venice, Italy, May 2003.

[158] M. Zhou and G.I.N. Rozvany. On the validity of ESO type methods in topology optimization. *Struct. Multidisc. Optim.*, 21:80–83, 2001.

[159] T. Borrvall and J. Petersson. Topology optimization using regularized intermediate density control. *Comput. Methods Appl. Mech. Engrg.*, 190:4911–4928, 2001.

[160] L. Ambrosio and G. Buttazzo. An optimal design problem with perimeter penalization. *Calculus of Variations and Partial Differential Equations*, 1:55–69, 1993.

[161] P. Duysinx. Layout optimization: A mathematical programming approach. Technical Report DCAMM Report No. 540, Technical University of Denmark, 1997.

[162] M. Beckers. Methodes du perimetre et des filtres pour l'optimisation topologique en variable discretes. Technical Report Technical Report OF-38, LTAS, University of Li'ege, 1996.

[163] J. Petersson and O. Sigmund. Slope constrained topology optimization. *Int. J. Numer. Meth. Engng.*, 41:1417–1434, 1998.

[164] T.P. Poulsen. A new scheme for imposing a minimum length scale in topology optimization: The MOLE method. In *Proceedings of the Fourth World Congress of Structural and Multidisciplinary Optimization*, Dalian, China, June 4-8 2001.

[165] O. Sigmund. *Design of material structures using topology optimization*. PhD thesis, Technical University of Denmark, 1994.

[166] G.K. Ananthasuresh, S. Kota, and Y. Gianchandani. A methodical approach to the design of compliant micromechanisms. In *Solid-state sensor and actuator workshop*, pages 189–192, 1994.

[167] C.B.W. Pedersen, T. Buhl, and O. Sigmund. Topology synthesis of large-displacement compliant mechanisms. *Int. J. Numer. Meth. Engng.*, 2001.

[168] S. Nishiwaki, K. Saitou, S. Min, and N. Kikuchi. Topological design considering flexibility under periodic loads. *Struct. Multidisc. Optim.*, 19:4–16, 2000.

[169] G.K. Lau, H. Du, and M.K. Lim. Use of functional specifications as objective functions in topological optimization of compliant mechanism. *Comput. Methods Appl. Mech. Engrg.*, 190:4421–4433, 2001.

[170] S.P. Gurav, M. Langelaar, and F. van Keulen. Uncertainty-based design optimization of shape memory alloy microgripper using combined cycle-based alternating anti-optimization and nested parallel computing. In *Proceedings of the 6th World Congresses of Structural and Multidisciplinary Optimization*, Rio de Janeiro, Brazil, May 2005. Paper no. 181.

[171] S. Canfield and M. Frecker. Topology optimization of compliant mechanical amplifiers for piezoelectric actuators. *Struct. Multidisc. Optim.*, 20:269–279, 2000.

[172] E.C.N. Silva and S. Nishiwaki. Multi-flexible micromanipulator design by using topology optimization. In *Proceedings of SPIE Smart Structures and Materials 2003 - Modeling, Signal Processing, and Control Conference*, volume 5049, pages 483–494, San Diego, U.S.A., 2003.

[173] E.C.N. Silva, S. Nishiwaki, J.S.O. Fonseca, and N. Kikuchi. Optimization methods applied to material and flextensional actuator design using the homogenization method. *Comput. Methods Appl. Mech. Engrg.*, 172:241–271, 1999.

[174] O. Sigmund and S. Torquato. Design of smart composite materials using topology optimization. *Smart Materials and Structures*, 8:365–379, 1999.

[175] Y. Li, X. Xin, N. Kikuchi, and Saitou K. Optimal shape and location of piezoelectric materials for topology optimization of flextensional actuators. In *Proceedings of the Genetic Evolutionary Computation Conference*, San Francisco, CA., U.S.A., July 2001.

[176] H. Du, G.K. Lau, M.K. Lim, and J. Qui. Topological optimization of mechanical amplifiers for piezoelectric actuators under dynamic motion. *Smart Materials and Structures*, 9:788–800, 2000.

Appendix A

A brief introduction to topology optimization

This appendix presents a very brief introduction to topology optimization as a material distribution problem. This brief review stems mainly from the review papers of Eschenauer and Olhoff [149], Frecker [103] and the book of Bendsøe and Sigmund [4]. For a more detailed review, the interested reader is therefore referred to these works and their references. This approach is characterised by the constitutive tensor of a material being parameterized within a predefined design domain Ω in order to determine the material domain Ω_{mat}, such that a given objective function is optimized.

Two of the most popular material models which parameterise the constitutive tensor are the homogenization and the SIMP (Simple Isotropic Material with Penalization) methods. Of course, a number of alternative approaches have been proposed. For example [98, 150, 151].

The SIMP material model has become very popular in recent times. The SIMP (Simple Isotropic Material with Penalization) was originally independently proposed by Bendsøe [109] and Zhou and Rozvany [110].

The SIMP material model modifies the elasticity tensor by simply premultiplying by a density $0 \leq \rho \leq 1$, raised to a power p, with $p > 1$:

$$E_{ijkl} = \rho(\boldsymbol{x})^p E^0_{ijkl}, \tag{A.1}$$

where E^0_{ijkl} is the elasticity tensor of the solid base material. The volume, on the other hand, is linearly dependant on ρ:

$$v(\rho) = \int_\Omega \rho(\boldsymbol{x}) \mathrm{d}V. \tag{A.2}$$

The penalty power makes intermediate densities uneconomical, since the stiffness of regions with intermediate densities are significantly reduced, while volume is contributed to linearly.

If $p = 1$ in A.1, the problem is converted to one where the energy depends linearly on ρ. In [13], it is noted that this linear problem provides the "most relaxed" problem and provides a useful bound on the maximum structural efficiency. An example of this type of problem is the variable thickness sheet problem.

Although the SIMP model is often referred to as an artificial or fictitious model since it was argued that intermediate densities could not be physically interpreted (as they can in the homogenization method). However, it was shown in [152] that the SIMP model can indeed be considered a realistic material model if p satisfies:

$$p \geq \max\left\{\frac{2}{1-\nu^0}, \frac{4}{1+\nu^0}\right\} \text{ in 2-D,} \tag{A.3}$$

$$p \geq \max\left\{\frac{15(1-\nu^0)}{7-5\nu^0}, \frac{3(1-\nu^0)}{2(1-2\nu^0)}\right\} \text{ in 3-D.} \tag{A.4}$$

That is to say, materials constructed from composites (materials with microstructure) which satisfy the Hashin-Shtrikman bounds. The Hashin-Shtrikman bounds for two-phase materials impose limits on materials properties achievable by constructing materials with microstructure from two linear elastic materials.

The simplicity and ease of implementation of the SIMP material model has seen topology optimization being adopted by a significant number of different elasticity problems and even different fields and problems, including : vibration and dynamics [104, 153, 154], buckling [155], flow [156], Micro Electro Mechanical Systems (MEMS) and multiphysics problems [106, 138], and even wave propagation problems [157].

A typical material distribution topology optimization problem can be stated as: Find the subdomain Ω_{mat} with a limited volume ($\bar{v}$) in Ω which minimizes a given objective function f (for example compliance). In order to solve the problem as a material distribution problem, a density function ρ is introduced which is 1 in Ω_{mat} and 0 elsewhere. Mathematically, this problem can be written as:

$$\begin{aligned} &\min_{\rho} f(\rho) \\ &\text{subject to} : v(\rho) = \int_{\Omega} \rho \, \mathrm{d}V \leq \bar{v} \\ &\qquad\qquad : \rho(\boldsymbol{x}) = 0 \text{ or } 1, \ \forall \boldsymbol{x} \in \Omega \\ &\qquad\qquad : \text{Physical laws} \end{aligned} \tag{A.5}$$

These problems are mostly solved using the finite element method. The discrete form of the problem can therefore be written as:

$$\begin{aligned} &\min_{\boldsymbol{\rho}} f(\boldsymbol{\rho}) \\ &\text{subject to} : v(\boldsymbol{\rho}) = \frac{1}{v_\Omega} \sum_{i=1}^{Nel} \rho_i v_i \leq v^* \\ &\qquad\qquad : \rho_i = 0 \text{ or } 1, \ \forall i = 1, 2, \ldots, Nel \\ &\qquad\qquad : \text{Physical laws} \end{aligned} \tag{A.6}$$

where v^* is an upper bound on the permissible volume fraction and Nel is the number of elements in the finite element mesh.

Of course numerous other methods to solve topology optimization problems exist. Examples include:

- *Evolutionary methods* which are related to fully stressed design methods and typically involve the iterative addition of elements in regions where they are predicted to be effective and removal from ineffective areas. Typically sensitivity information is not required or used in these methods. Although these methods are usually relatively easy to implement, Eschenauer and Olhoff [149] warn that evolutionary structural optimization-type methods are heuristic and have been shown to fail for even simple problems [158].

- Employing *topological derivatives* and *bubble methods* extends the use of boundary variation shape optimization techniques to topology optimization. Principally, the sensitivity to the addition of an infinitesimally small hole (a change in topology) at a certain point in the design domain is estimated. The topological derivative is used where necessary to alter the topology, while standard shape optimization techniques are used to manipulate the interior and exterior boundary shapes.

  Level set methods have also become quite popular of late. Essentially, as explained by Bendsøe and Sigmund [4], the contours of a parameterized family of level-set functions are used to define and alter the boundaries of a structure.

  Although these methods are theoretically sound, they are rather complex and are difficult to implement. Furthermore, although they have been demonstrated on problems such as the minimum compliance problem, they are difficult to extend to practical problems such as compliant mechanism design.

- Since discrete (0-1) solutions are ultimately sought from the topology optimization routine, it seems attractive to tackle the problem using *discrete variables*. Easily implemented gradient-free optimization algorithms such as Genetic Algorithms (GA's) and Particle Swarm Optimization Algorithms (PSOA's) have previously been applied to problems in topology optimization. However, these methods have had little success since, due to the large scale of the problems, a restrictively large number of (relatively numerically expensive) function evaluations are required.

Once again, a more detailed survey of these methods can be found in for example [149, 4].

A.1 Implementional issues

There are several known implementational issues which need to be dealt with appropriately if topology optimization procedures are to yield sensible results. These issues include: *existence* of solution (*mesh dependency*), *checkerboarding*, *one-node connected hinges*, *non-uniqueness*, and *local minima*. In this section, some of the work that has been published in open literature to deal with these issues, will be highlighted.

A.1.1 Mesh dependency

Problem (A.5) is well know to lack solution in general. A somewhat simplified explanation for this is that for a given design, with known volume, allowing the addition of new holes

(without increasing the volume) generally increases the efficiency of the allowable optimal design. More specifically, the set of feasible designs is not closed. This nonexistence problem (mesh dependence in the discrete case (A.6)) can be overcome by either relaxation or by restriction of the design domain.

Problem relaxation involves expanding the set of permissible designs to achieve existence. Bendsøe and Kikuchi [107] famously relaxed the problem by permitting composite microstructure using a homogenization method. The homogenization method describes global behaviour in terms of a microscopic base cell. Using this method, each elements effective density is allowed to vary such that $0 \leq \rho_i \leq 1$, $\forall i = 1, 2, \ldots Nel$, based on the parameterization of the base cell. Using this procedure however, can result in large areas of intermediate density which can be physically interpreted, but are difficult to manufacture.

Methods do exist to explicitly penalize intermediate densities, e.g. see [13, 159]. The problem with this explicit penalization of intermediate densities is however, that one is essentially reverting back to the problem in (A.6) which lacks solution!

More detail on topology optimization using homogenization methods can be found in Section 7.5.1. The detail of this method will therefore not be repeated here since the focus of this study is on the SIMP method.

The other method to overcome the non-existence problem is to restrict the set of admissible designs. Restriction methods involve decreasing the size of the set of feasible designs. In doing so, the set of all possible designs is sufficiently closed.

For detailed reviews of restriction methods, the reader is referred to [4, 13]. Since many of these methods also have the effect of reducing checkerboarding, some details of methods to deal with the mesh dependency problem will be presented here.

Perimeter control

The basic idea of this method is to (as the name suggests) restrict the perimeter of the solid domain Ω_{mat}. Roughly speaking, the perimeter is the sum of the perimeters of all the holes and the perimeter of boundary. Importantly, existence to topology optimization problems with a restriction on the perimeter was proven by Ambrosio and Buttazzo [160].

Haber *et al.* developed the first numerical implementation of this method. They impose a constraint on the total variation, which is in fact the perimeter of the solid domain if $\rho = 1$ in Ω_{mat} and $\rho = 0$ elsewhere. The discrete form of the total variation is:

$$P = \sum_{k=1}^{K} l_k \left(\sqrt{< \rho >_k^2 + \epsilon^2} - \epsilon \right), \tag{A.7}$$

where $< \rho >_k$ is the jump in material density over element interface k of length l_k. $K \approx 2Nel$ is the number of element interfaces and ϵ is a small number used to produce a differential function in place of the absolute value. Other workers who have made contributions are Duysinx [161] for continuous variables and Beckers [162] who worked with discrete variables. This method results in the inclusion of only one additional constraint which can easily be accommodated by general purpose optimizers such as MMA.

A reported drawback of this method is that that perimeter constraint is relatively difficult to approximate, resulting in fluctuations in the design variables. This is reported to be related to the choice of asymptotes of MMA [4]. These implementational issues were alleviated by an inner loop procedure for the relatively inexpensive perimeter approximation by Duysinx [161]. Furthermore, the choice of the actual bounding value is not easily physically justifiable.

Global gradient constraint

Bendsøe [139] proved existence of solution when including this bound in topology optimization problems. The global constraint simply involves imposing a bound on the norm of the ρ function in the Sobolov space $H^1(\Omega)$,

$$||\rho||_{H^1} = \left(\int_{Omega} (\rho^2 + |\nabla \rho|^2 \mathrm{d}V) \right)^{1/2} \leq M. \tag{A.8}$$

This method also only involves one additional constraint function, however Bendsøe and Sigmund [4] report that implementation of A.8 also involves some experimentation with a range of values for bound M to achieve acceptable results.

Local gradient constraint

Petersson and Sigmund [163] proved existence of solution for, as well as numerically implemented, a scheme introducing local gradient constraints. Point-wise bounds on the spacial derivatives of function ρ are imposed:

$$|\frac{\partial \rho}{\partial x_i}| \leq G, i = 1, 2, 3 \text{ (in three dimensions)}. \tag{A.9}$$

This scheme (which essentially constrains the L^∞ norm of the gradient of ρ) has the advantage that the gradient constraint provides a well defined length scale. That is to say, the transition from solid, to void, back to solid requires a distance of at least $2/G$. However, implementation of this scheme results in (up to) $2Nel$ additional constraints for the optimization problem, making large scale implementation difficult.

MOLE method

Recently a scheme named 'MOLE' (MOnoticity based minimum LEngth scale) has been proposed by Poulsen [164]. In essence, the idea is to pass a circular filter over the design domain and measure the monotonicity of the density function (horizontally, vertically and at +/- 45°). If a non-monotonic density distribution is detected at a smaller length scale than desired, a constraint function becomes non-zero. A permissible tolerance is placed on this function, resulting in only one additional constraint being added to the optimization problem.

Filtering of elemental densities

In a discrete implementation, this scheme modifies each elements density as some weighted sum of the surrounding elements within a certain distance [4]. Features larger than the filter size are implicitly penalised, since any non-uniformities within the filter area will result in a 'grey' element which is uneconomical in the SIMP model.

Implementation requires sensitivities of each element to take into account the mutual energy of elements within the filter radius. Therefore, although no additional constraints are added to the optimization problem, but bookkeeping in the computation of sensitivities may be somewhat involved.

Filtering sensitivities

A method which has been widely used by numerous authors is to filter the sensitivity information of the optimization problem. Although the method is purely heuristic, it is extremely efficient and has been shown to provide very good results for a wide range of problems, for examples see [4], with very little additional computational expense. Furthermore no additional constraints are added to the optimization problem, and therefore standard optimality criteria methods can be used.

The filter was originally proposed by Sigmund [100, 165] and not only does this scheme impose a sensible length scale on the problem but also eliminates checkerboarding. The scheme works by modifying the sensitivities as follows:

$$\frac{\hat{\partial} f}{\partial \rho_k} = (\rho_k)^{-1} \frac{1}{\sum_{i=1}^{Nel} \hat{H}_i} \sum_{i=1}^{Nel} \hat{H}_i \rho_i \frac{\partial f}{\partial \rho_i}, \tag{A.10}$$

where a linear convolution operator $\hat{H}_i$ can be written as

$$\hat{H}_i = r_{\min} - \text{dist}(k,i), \{i \in Nel | \text{dist}(k,i) \leq r_{\min}\}, k = 1, 2, \ldots, Nel, \tag{A.11}$$

and $\text{dist}(k,i)$ is the distance between the centroid of elements k and i, and $\hat{H}_i$ is zero outside the filter area.

A.1.2 Checkerboarding, one-node connected hinges

The checkerboarding phenomena is described in detail in Chapter 7, and therefore only a condensed treatment will be presented here. The checkerboarding problem is characterised by material distributions in "optimal topologies" being distributed in alternating solid and void elements. Checkerboarding is largely as a result of poor numerical modelling of this spurious material distribution, as shown by Díaz and Sigmund [14] and Jog and Haber [102]. In essence, the numerical behaviour of this material distribution is over-stiff.

The one-node connected hinge is characterised by four elements surrounding a node, where two diagonally opposite elements are solid and the other two are void. Although it is reported

that the mesh-independency sensitivity filtering scheme also eliminates checkerboarding, one-node connected hinges are still possible, and are in fact somewhat common when applied in the design of compliant mechanisms. The reason is that in compliant mechanism design, solid state hinges are employed to achieve the required motion and the numerical model of a on-node hinge employing standard Q4 elements is ideal (if unrealistic and inaccurate) since it offers zero resistance to bending.

Methods to overcome the problems of checkerboarding or one-node hinges (or both) are numerous, and therefore only selected popular methods with be presented here.

Higher order elements

It was shown by Díaz and Sigmund [14] and by Jog and Haber [102] that checkerboarding is to a large extent eliminated when higher order (Q8 or Q9 planar) elements are employed with the homogenization material model. However, as was shown in Chapter 7, checkerboarding is only prevented in the SIMP model for a limited range of values for the penalty power p. A significant drawback is that higher order elements are significantly more numerically expensive than standard elements.

Patches

An alternative is to eliminate checkerboarding in a patch of elements. Patches are comprised of four regular elements with a common node in the centre of the patch. The complete mesh is therefore made up of $P_x \times P_y$ patches or $2P_x \times 2P_y$ elements. Each patch of four elements can be viewed as a single "super-element".

Four orthogonal basis functions are defined for the patch, similar to those described in Section 5.5.2, one of which defines a pure checkerboard pattern. The ρ function is then restricted to lie within a reduced, checkerboard-free space. This is achieved by, for each patch, modifying the updated design variables by removing the component associated with the pure checkerboard basis function [4].

Alternatively wavelet methods can be employed to directly work in a space without checkerboarding [98, 151]. It was shown that this method can be used to prevent checkerboarding as well as to obtain some geometry control.

Filters

The scheme employed to impose mesh-independency, introduced by Sigmund [100] also efficiently alleviates the checkerboarding problem.

NoHinge

Poulsen [15] developed a simple scheme to avoid the formation of one-node connected hinges and checkerboard patterns. This scheme results in a single additional constraint based on a

measure of non-monotonicity of density around each interior node in the mesh. This method is the basis of the new scheme developed in Section 5.5.2.

Other Methods

Most of the restriction methods described in the previous section also alleviate the effects of checkerboarding.

A.1.3 Other complications

Other common complications in topology optimization problems are multiple (local) optima and non-uniqueness. If one observes the many different optimal solutions which have been published for, for example the MBB beam problem, it is clear that there are many local optima present in these problems. This is due to the fact that most topology optimization problems are non-convex. A popular method to alleviate non-convexity is the use of continuation methods, in which problems are gradually changed from (artificial) convex or nearly convex problems to the original non-convex problem. An example would be raising the penalty exponent p from 1 to higher values gradually, or gradually raising the value of filter radius until the desired value is reached.

Problems with multiple optimal solutions (with the same objective value) are termed non-unique. An example commonly cited is that of a structure under uniaxial tension, in which only the cross-sectional area is of importance and not the topology. The only sensible way to deal with this problem is to impose manufacturing preference constraints.

A.2 Compliant mechanism design

Since the ultimate application of the scheme developed in this investigation, is a piezoelectrically driven mirror scanning device designed using topology optimization, a brief review of previous work in the field is appropriate.

This review is not meant to be an exhaustive review, but is simply meant to give some background to problems previously considered in this field. Again, for a more comprehensive review the reader is referred to the book of Bendsøe and Sigmund [4] and to the review article by Frecker [103].

Compliant mechanisms achieve their mobility via the solid-state flexibility of different regions (components) within a single connected structure[1]. The fact that they are solid-state makes their use especially attractive when piezoelectric actuators are used. Piezoelectric actuators are capable of relatively small strokes (usually in the order of μm), which can easily be lost to any play in the system.

Original works in the field are credited to Ananthasuresh *et al.* [166] and Sigmund [100]. Since then, numerous works have appeared, e.g. see [101, 138]. Mechanisms able to gen-

[1] Of course the mechanism itself can include multiple parts e.g. actuation mechanism connected to a mechanical amplifier.

erate specific prescribed paths have been developed by (for example Pedersen *et al.* [167]. Optimization of mechanisms for dynamic response has been considered by for example Min and Kikuchi [168]. In most of these works, the output load is modelled using a spring with specific stiffness against which the mechanism works.

In [169], instead of using a spring for the output to work against, various alternative function specifications are investigated. Examples include, mechanical advantage, geometrical advantage and work ratio.

Topology optimization of smart structures is now specifically considered, especially those employing piezoelectric actuation. Notably, far less attention has been paid to other smart materials, such as shape memory alloys [170].

Canfield and Frecker [171] used a ground structure approach to design mechanical amplifiers for piezoelectric stack actuators by maximizing geometrical advantage or maximizing mechanical efficiency. The ground structure approach results in relatively sparse structures which are not easily manufacturable.

In Silva and Nishiwaki [172] a micromanipulator is designed using the homogenization topology optimization method. This multi-flexible structure requires various prescribed output displacements at different points in the domain for various excitations due to piezoelectric actuators.

Silva *el al.* [173] also used the homogenization method in the design of piezoelectric composite material microstructures. They maximize given performance measures by designing a material microstructure with prescribed material properties. Sigmund and Torqato [174] employed a similar procedure to design and manufacture piezoelectric material microstructures, except that the SIMP method is employed.

In Li *et al.* [175], the optimal shape and location of piezoelectric materials within the (optimal) compliant mechanism were generated. The placement of the piezoelectric material was performed in an outer loop, optimized with a G.A. and the compliant mechanism optimization carried out (for fixed location) in an inner loop.

Generally, mechanisms obtained using linear modelling in the topology optimization infrastructure do not behave optimally when subjected to large input/output displacements. For these applications geometrically non-linear modelling is required to generate optimal compliant mechanisms which produce the required motion. This problem was considered by for example Bruns *et al.* [137] and Pedersen *et al.* [167]. Non-linear modelling is not necessary for our applications driven by a piezoelectric actuator since free strains in the stacks employed are typically in the order of $0.1-0.2\%$.

Finally, topology optimization of mechanical amplifiers subjected to dynamic motion was considered by [176].

Appendix B

Additional plate and shell results

In order to maintain the conciseness of Chapter 6, only the most important and immediately relevant results were presented within the chapter itself. In this appendix supplemental results are presented which corroborate the evidence and support the conclusions drawn during the course of the investigation. The additional results that are referred to, but not explicitly given in Chapter 6, are therefore presented herein.

B.1 Additional membrane results

Firstly, the supplemental membrane results are given. For details of the considered problem, the reader is referred to Section 6.5.1.

B.1.1 MBB beam

The geometry, material properties, restraints and loading are all depicted in Figure 6.6. Although symmetry is used to model the structure, the complete topology is reported. In total 2700 square elements are used, 90 elements along the length of the finite element model, $L/2$ and 30 elements in the height h. Of course, since only membrane components are evaluated, only the single layer material model is tested. The available volume fraction is half of the design domain.

Figure B.1 depicts the convergence histories for the topologies shown in Figure 6.8. In order to stabilize the convergence, the penalty exponent is stepped from 1 to 3 as shown on the convergence history plots. Also, the objective is normalized with respect to the starting value of compliance in order to improve the problem scaling.

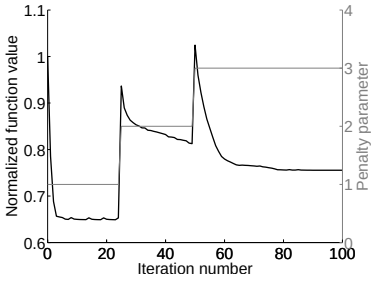

(a) Q4 element. (same for all α)

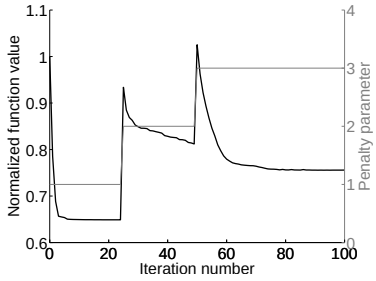

(b) Q4γ element, $\alpha = 0$.

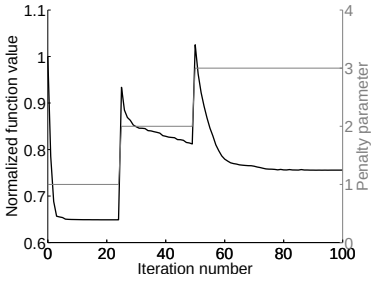

(c) Q4γ element, $\alpha = 10^{-6}$.

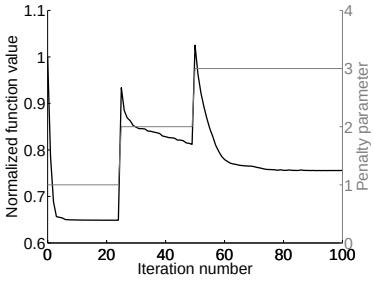

(d) Q4γ element, $\alpha = 10^{-4}$.

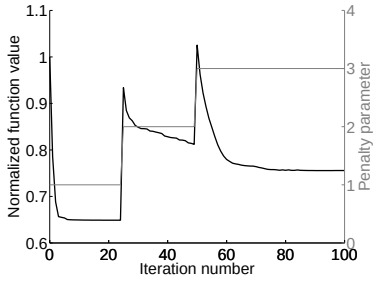

(e) Q4γ element, $\alpha = 10^{-2}$.

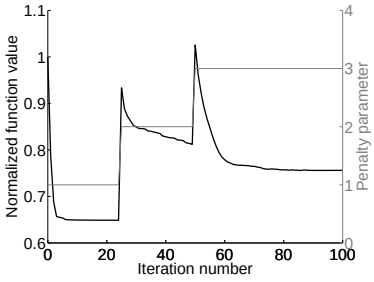

(f) Q4γ element, $\alpha = 10^{0}$.

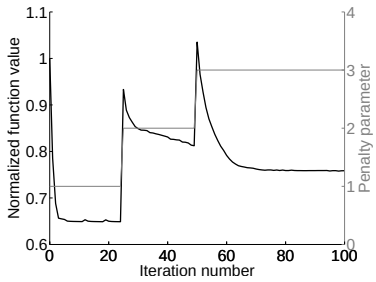

(g) Q4γ element, $\alpha = 10^{2}$.

Figure B.1: Convergence histories for MBB beam for various values of α.

B.2 Additional plate results

In this section, supplemental plate results are detailed. For more information about the considered problems, see Section 6.5.3 herein.

B.2.1 Simply supported square plate with centre point load

The geometry and constraints for the first plate problem are depicted in Figure 6.9(a). The problem consists of a square plate which is simply supported, and subjected to a unit point load applied to the center of the plate. Three material models are analyzed, namely single layer, ribbed and honeycomb material models.

The results for this problem are depicted in Figures B.2 to B.7. Figures B.2 and B.3 depict respectively the optimal topologies and convergence histories for the thin and thick single layer models. Figures B.4 and B.5 represent the optimal topologies for the thin and thick ribbed material models, with corresponding convergence histories. The results for the thin and thick honeycomb material models are depicted in Figures B.6 and B.7, respectively.

The tables accompanying each figure, tabulate the difference in compliance between the optimal topologies, analyzed using the three plate elements utilized in this study. The values represent the percentage difference between the compliance of the optimal topology computed with a given element, and the compliance calculated using the remaining two elements. Of course, there is no difference between the compliance of the optimal topology calculated with any element and itself, accounting for the zero terms on the diagonal of each table.

Single layer material model

Figure B.2 illustrates that similar topologies are computed using each of the different elements when considering the thin simply supported plate, with single layer material model. Table B.1, further shows that the solutions obtained from the two Mindlin-Reissner elements (in particular the ANS element) are marginally better than the result obtained using the DKQ element. A possible explanation for the slight improvement on the DKQ results, is that the regions of intermediate density (which contribute little to the compliance) are less pronounced in the two Mindlin-Reissner elements. The correctness of these results may be confirmed when compared to previously published results for similar problems [3, 115, 4].

Figure B.3 contains the results for the thick single layer problem. In this case the topology obtained using the DKQ element differs from the topologies obtained using the two Mindlin-Reissner elements. Since the DKQ element is shear rigid, the thick optimal topology is identical to the thin result as expected. Table B.2 shows, the compliance of the structure generated using DKQ elements has approximately 18% higher compliance (lower stiffness) than the topology computed with ANS elements, when both are modelled using ANS elements. The DKQ result has a 24% higher compliance than the result obtained with SRI elements, when both are analysed using SRI elements. Although the 18% and 24% differences cannot directly be compared since the percentage differences are calculated relative

	Optimal topology generated using:		
	DKQ	ANS	SRI
Analysed with DKQ	0.0000	-0.4871	-0.0641
Analysed with ANS	0.6021	0.0000	0.2734
Analysed with SRI	0.7677	-0.1193	0.0000
Constraint value	5.5924e-05	-4.4603e-05	-6.8271e-05

Table B.1: Percentage difference: Simply supported square plate subjected to center point load, single layer model, $t = 0.01$.

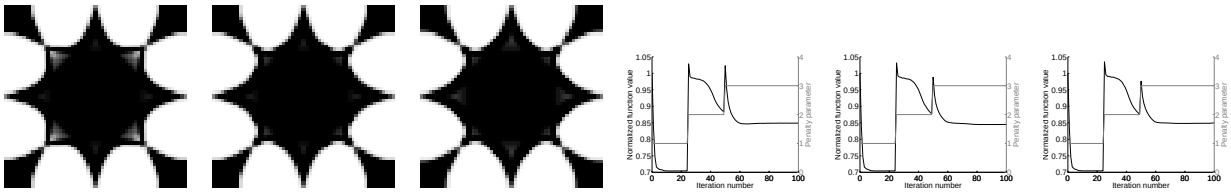

(a) DKQ. (b) ANS. (c) SRI. (d) DKQ. (e) ANS. (f) SRI.

Figure B.2: Optimal topologies of a simply supported square plate subjected to center point load, single layer model, $t = 0.01$: (a)-(c) optimal topologies, (d)-(f) convergence histories.

to different designs, the discrepency is significant. This difference is likely as a result of the SRI element being softer than the ANS elements in transverse shear.

	Optimal topology generated using:		
	DKQ	ANS	SRI
Analysed with DKQ	0.0000	1.3109	3.1641
Analysed with ANS	17.5832	0.0000	1.1297
Analysed with SRI	24.3415	-0.4341	0.0000
Constraint value	5.5924e-05	1.1389e-05	-7.5900e-06

Table B.2: Percentage difference: Simply supported square plate subjected to center point load, single layer model, $t = 0.1$.

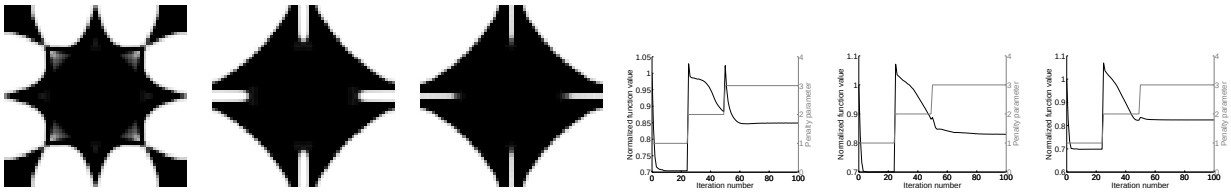

(a) DKQ. (b) ANS. (c) SRI. (d) DKQ. (e) ANS. (f) SRI.

Figure B.3: Optimal topologies of a simply supported square plate subjected to center point load, single layer model, $t = 0.1$: (a)-(c) optimal topologies, (d)-(f) convergence histories.

Ribbed material model

Figures B.4 and B.5, together with Tables B.3 and B.4 indicate that the ribbed design solutions are similar for the thin and thick structures. The shape of the thick Mindlin-Reissner solutions differ slightly from the thin results, but the difference in compliance, presented in Table B.4, is insignificant.

	Optimal topology generated using:		
	DKQ	ANS	SRI
Analysed with DKQ	0.0000	-0.1651	-0.2534
Analysed with ANS	0.1721	0.0000	-0.0868
Analysed with SRI	0.2514	0.0823	0.0000
Constraint value	7.0194e-05	2.4505e-05	-2.5642e-06

Table B.3: Percentage difference: Simply supported square plate subjected to center point load, ribbed model, $t = 0.01$.

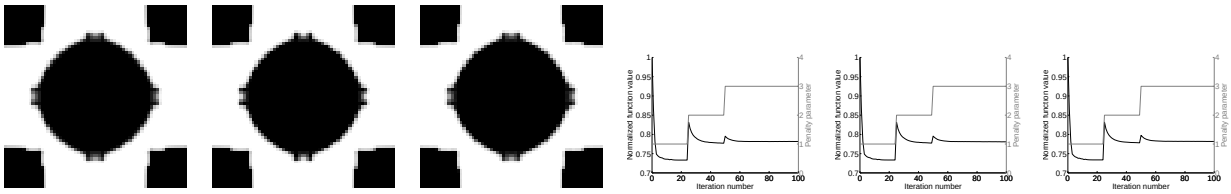

(a) DKQ. (b) ANS. (c) SRI. (d) DKQ. (e) ANS. (f) SRI.

Figure B.4: Optimal topologies of a simply supported square plate subjected to center point load, ribbed model, $t = 0.01$: (a)-(c) optimal topologies, (d)-(f) convergence histories.

	Optimal topology generated using:		
	DKQ	ANS	SRI
Analysed with DKQ	0.0000	1.4849	1.5135
Analysed with ANS	0.4956	0.0000	0.0404
Analysed with SRI	0.5351	-0.0030	0.0000
Constraint value	7.0194e-05	-1.1443e-04	4.4419e-05

Table B.4: Percentage difference: Simply supported square plate subjected to center point load, ribbed model, $t = 0.1$.

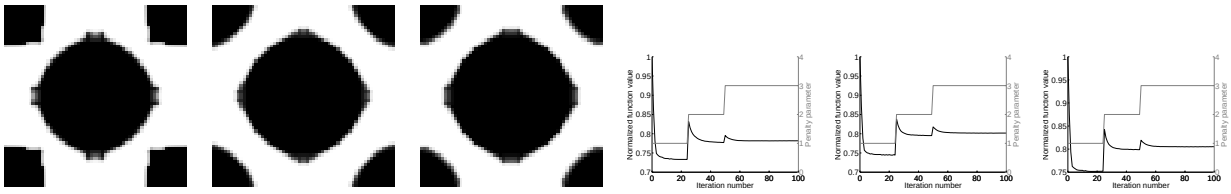

(a) DKQ. (b) ANS. (c) SRI. (d) DKQ. (e) ANS. (f) SRI.

Figure B.5: Optimal topologies of a simply supported square plate subjected to center point load, ribbed model, $t = 0.1$: (a)-(c) optimal topologies, (d)-(f) convergence histories.

Honeycomb material model

Considering the honeycomb layered model, the Mindlin-Reissner elements recover the same topology as the Kirchhoff element for the thin structure. For the thick plate however, although the percentage difference in function values presented in Table B.6 are very small, the optimal topologies calculated using using each element differ. What is more, Table B.6 confirms that the optimal topology generated with each element, is superior to the topologies calculated using the remaining two elements. This illustrates that the 'optimal' (shape or) topology is dependent on which element is employed in the finite element analysis. Again, the assumption is that the difference, especially between the two Mindlin-Reissner elements is due to the ANS element being slightly stiffer than the SRI element in transverse shear.

	Optimal topology generated using:		
	DKQ	ANS	SRI
Analysed with DKQ	0.0000	0.0006	0.0004
Analysed with ANS	-0.0005	0.0000	-0.0002
Analysed with SRI	-0.0003	0.0002	0.0000
Constraint value	1.3423e-04	-1.7928e-04	-1.8889e-04

Table B.5: Percentage difference: Simply supported square plate subjected to center point load, honeycomb model, $t = 0.01$.

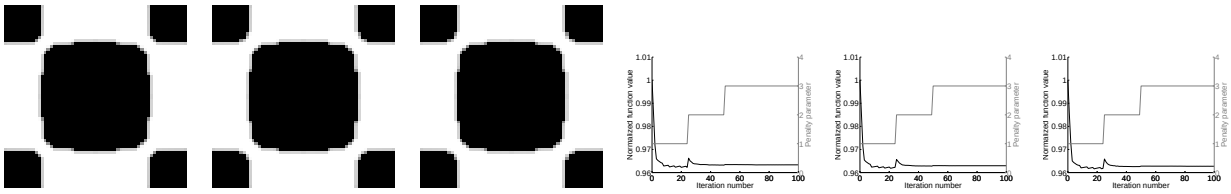

(a) DKQ. (b) ANS. (c) SRI. (d) DKQ. (e) ANS. (f) SRI.

Figure B.6: Optimal topologies of a simply supported square plate subjected to center point load, honeycomb model, $t = 0.01$: (a)-(c) optimal topologies, (d)-(f) convergence histories.

	Optimal topology generated using:		
	DKQ	ANS	SRI
Analysed with DKQ	0.0000	0.1873	0.5094
Analysed with ANS	0.1218	0.0000	0.0522
Analysed with SRI	0.4893	0.1351	0.0000
Constraint value	1.3423e-04	1.6512e-04	-9.2279e-05

Table B.6: Percentage difference: Simply supported square plate subjected to center point load, honeycomb model, $t = 0.1$.

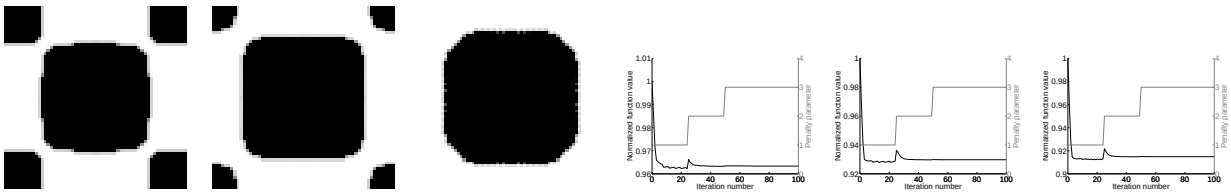

(a) DKQ. (b) ANS. (c) SRI. (d) DKQ. (e) ANS. (f) SRI.

Figure B.7: Optimal topologies of a simply supported square plate subjected to center point load, honeycomb model, $t = 0.1$: (a)-(c) optimal topologies, (d)-(f) convergence histories.

B.2.2 Clamped square plate with centre point load

The geometry for this problem is depicted in Figure 6.9(b). The load considered is again a unit point load applied to the center of the plate. This problem has been considered by a number of authors [4, 115], and our thin plate results compare favorably with theirs.

Single layer material model

The results for this problem are contained in Figures B.8 to B.13, and Tables B.7 to B.12. Figures B.8 and B.9, together with Tables B.7 and B.8 present the results for the thin and thick single layer models, respectively. Figures B.10 and B.11 and Tables B.9 and B.10 present the analysis thin and thick ribbed material models. The results for the thin and thick honeycomb material models are presented in Figures B.12 and B.13 with corresponding analysis in Tables B.11 and B.12, respectively.

From Figure B.8 and Table B.7 it is evident that, for the thin single layer material model, almost identical topologies are achieved for all elements. Although there is no visible difference between the three topologies, the negative values in the third column of Table B.7 indicate that the SRI result is marginally superior. The thick plate model on the other hand, results in slightly different topologies when Mindlin-Reissner elements are used compared to the result with the DKQ element. The finite element model is highly constrained, which could explain the slightness in difference between the thin and thick results. Nevertheless, the effect on the compliance is significant, with a 14% improvement on the thin topology's compliance compared to the result using ANS elements, when analysed with ANS elements and a 37% improvement when compared to the SRI results, analysed with SRI elements. Again, although the 14% and 37% difference cannot be directly compared (because the differences are computed with respect to different optimal topologies) the indication is that the ANS elements are slightly more stiff in transverse shear than the SRI elements.

	Optimal topology generated using:		
	DKQ	ANS	SRI
Analysed with DKQ	0.0000	-0.1317	-0.3028
Analysed with ANS	0.1733	0.0000	-0.1513
Analysed with SRI	0.6954	0.7259	0.0000
Constraint value	-5.5042e-05	3.1765e-05	-7.8998e-05

Table B.7: Percentage difference: Clamped square plate subjected to center point load, single layer model, $t = 0.01$.

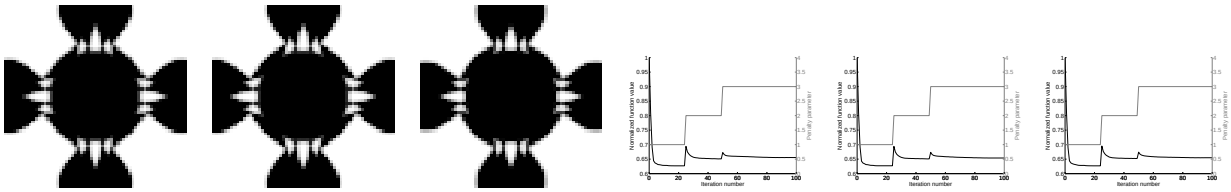

(a) DKQ. (b) ANS. (c) SRI. (d) DKQ. (e) ANS. (f) SRI.

Figure B.8: Optimal topologies of a clamped square plate subjected to center point load, single layer model, $t = 0.01$: (a)-(c) optimal topologies, (d)-(f) convergence histories.

	Optimal topology generated using:		
	DKQ	ANS	SRI
Analysed with DKQ	0.0000	1.3371	2.4424
Analysed with ANS	13.9028	0.0000	-0.0229
Analysed with SRI	37.0471	0.8543	0.0000
Constraint value	-5.5042e-05	-7.2254e-05	8.2104e-06

Table B.8: Percentage difference: Clamped square plate subjected to center point load, single layer model, $t = 0.1$.

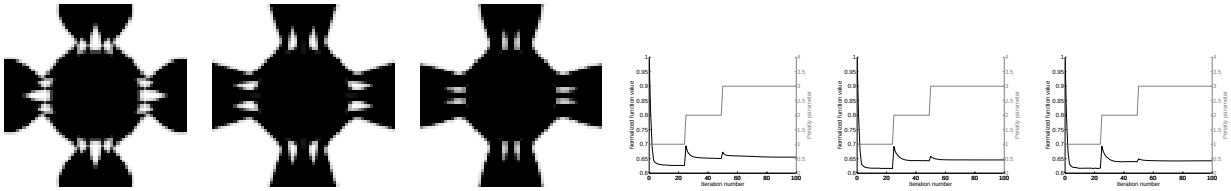

(a) DKQ. (b) ANS. (c) SRI. (d) DKQ. (e) ANS. (f) SRI.

Figure B.9: Optimal topologies of a clamped square plate subjected to center point load, single layer model, $t = 0.1$: (a)-(c) optimal topologies, (d)-(f) convergence histories.

Ribbed material model

For the ribbed material model, the thin and thick structures result in the same topologies for all elements as depicted in Figures B.10 and B.11. However, again the shape of the Mindlin-Reissner results differs slightly from the DKQ results for the thick plate. The values of compliance for the thin and thick plates are again similar for all elements, as shown in Tables B.9 and B.10.

	Optimal topology generated using:		
	DKQ	ANS	SRI
Analysed with DKQ	0.0000	0.0028	0.0115
Analysed with ANS	-0.0026	0.0000	0.0099
Analysed with SRI	-0.0098	-0.0069	0.0000
Constraint value	7.4645e-05	-2.9307e-05	-4.0355e-05

Table B.9: Percentage difference: Clamped square plate subjected to center point load, ribbed model, $t = 0.01$.

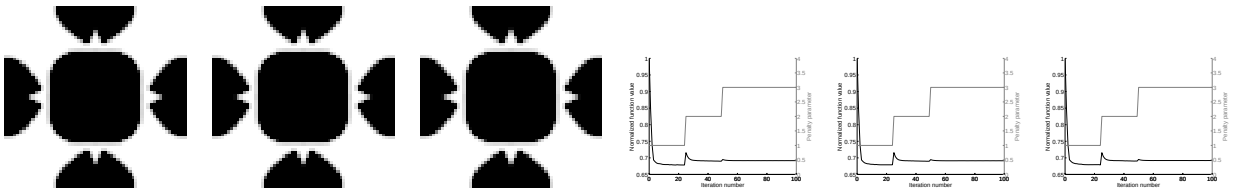

(a) DKQ. (b) ANS. (c) SRI. (d) DKQ. (e) ANS. (f) SRI.

Figure B.10: Optimal topologies of a clamped square plate subjected to center point load, ribbed model, $t = 0.01$: (a)-(c) optimal topologies, (d)-(f) convergence histories.

	Optimal topology generated using:		
	DKQ	ANS	SRI
Analysed with DKQ	0.0000	0.5273	0.5113
Analysed with ANS	0.1536	0.0000	0.0024
Analysed with SRI	0.2054	0.0593	0.0000
Constraint value	7.4645e-05	-9.2086e-05	7.4218e-05

Table B.10: Percentage difference: Clamped square plate subjected to center point load, ribbed model, $t = 0.1$.

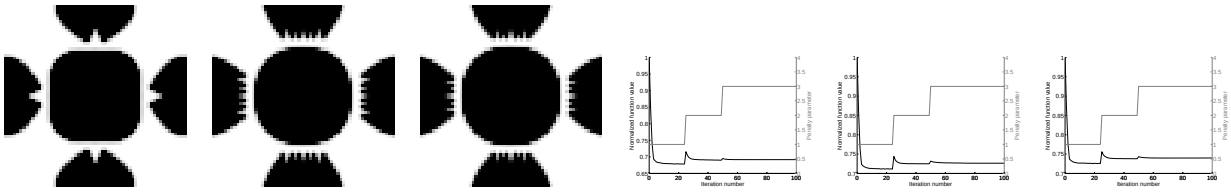

(a) DKQ. (b) ANS. (c) SRI. (d) DKQ. (e) ANS. (f) SRI.

Figure B.11: Optimal topologies of a clamped square plate subjected to center point load, ribbed model, $t = 0.1$: (a)-(c) optimal topologies, (d)-(f) convergence histories.

Honeycomb material model

Although in the case of the honeycomb material model, the optimal topologies for the thick plate generated using Mindlin-Reissner elements (see Figure B.13) are different to the results for the thin plate (depicted in Figure B.12), the result on the compliance is modest. However, the compliance results presented in Table B.12 do confirm that the optimal topology calculated using Mindlin-Reissner elements is lower than the DKQ topology for thick plates, whereas the DKQ result is indeed superior for thin plate problems.

	Optimal topology generated using:		
	DKQ	ANS	SRI
Analysed with DKQ	0.0000	-0.0060	0.0057
Analysed with ANS	0.0063	0.0000	0.0119
Analysed with SRI	-0.0058	-0.0120	0.0000
Constraint value	-5.9377e-05	-1.8208e-04	-1.3014e-04

Table B.11: Percentage difference: Clamped square plate subjected to center point load, honeycomb model, $t = 0.01$.

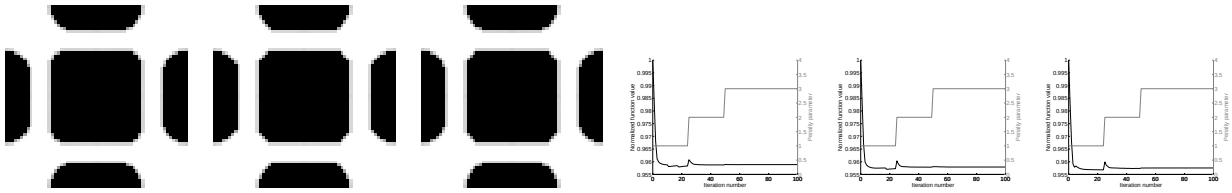

(a) DKQ. (b) ANS. (c) SRI. (d) DKQ. (e) ANS. (f) SRI.

Figure B.12: Optimal topologies of a clamped square plate subjected to center point load, honeycomb model, $t = 0.01$: (a)-(c) optimal topologies, (d)-(f) convergence histories.

	Optimal topology generated using:		
	DKQ	ANS	SRI
Analysed with DKQ	0.0000	0.2895	0.3975
Analysed with ANS	0.6686	0.0000	0.0097
Analysed with SRI	1.2910	0.0929	0.0000
Constraint value	-5.9377e-05	7.6439e-06	-1.0764e-04

Table B.12: Percentage difference: Clamped square plate subjected to center point load, honeycomb model, $t = 0.1$.

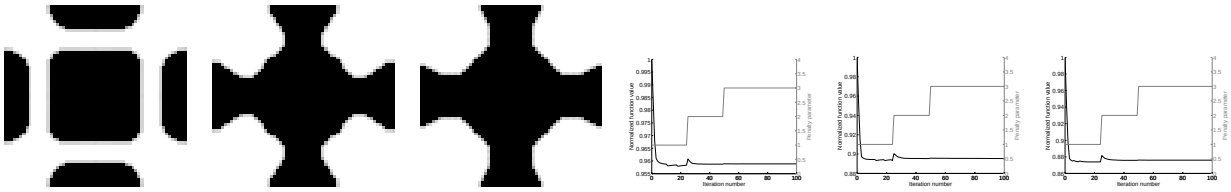

(a) DKQ. (b) ANS. (c) SRI. (d) DKQ. (e) ANS. (f) SRI.

Figure B.13: Optimal topologies of a clamped square plate subjected to center point load, honeycomb model, $t = 0.1$: (a)-(c) optimal topologies, (d)-(f) convergence histories.

B.2.3 Corner supported square plate with centre point load

The final plate geometry with restraints is depicted in Figure 6.9(c). It represents a corner supported plate (i.e. transverse displacement is constrained at the four corner nodes only). For this problem, the first load case considered, is again a center point load as before. Again the single layer, ribbed and honeycomb material models are analyzed.

Figures B.14 to B.19 with corresponding Tables B.13 to B.18 present the results for the corner supported square plate subjected to a center point load, for the single layer, ribbed and honeycomb material models.

Single layer material model

In Figure B.14 the optimal topologies for the thin, single layer material model are depicted. Once again, the topologies of all three elements are very similar. Although the SRI elements convergence history shows that some numerical problems were encountered during the optimization process, the final topology is not significantly affected. Albeit similar topologies are computed for the DKQ and ANS elements, Table B.13 indicates that the DKQ topology shows a 1% improvement over the optimal ANS results, when analysed using ANS elements.

	Optimal topology generated using:		
	DKQ	ANS	SRI
Analysed with DKQ	0.0000	1.2686	1.8995
Analysed with ANS	-1.0090	0.0000	0.5854
Analysed with SRI	2.1438	2.5740	0.0000
Constraint value	-5.2618e-05	-5.2688e-05	-3.4714e-05

Table B.13: Percentage difference: Corner supported square plate subjected to center point load, single layer model, $t = 0.01$.

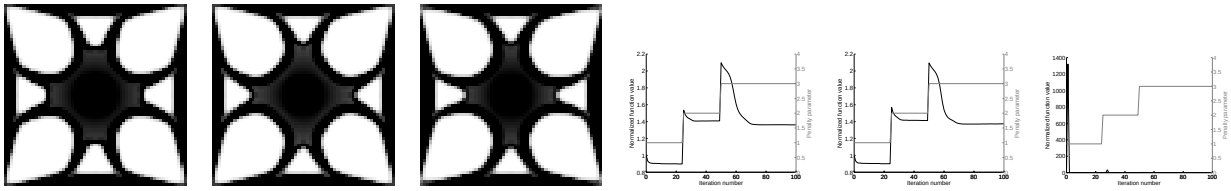

(a) DKQ. (b) ANS. (c) SRI. (d) DKQ. (e) ANS. (f) SRI.

Figure B.14: Optimal topologies of a corner supported square plate subjected to center point load, single layer model, $t = 0.01$: (a)-(c) optimal topologies, (d)-(f) convergence histories.

The results for the thick single layer material model are depicted in Figure B.15. In this case, the SRI result is distinctly different from the results using the other two elements.

Table B.14 shows that the compliance of the SRI result is approximately 4.5% lower than the DKQ result when both designs are analysed with DKQ elements and approximately 8.5% better than the ANS result when analysed using ANS elements. In this specific case the SRI element clearly realised the best design. This is again, probably due to the SRI element being 'softer' in transverse shear than the other two elements, which results in the optimizer searching different parts of the design domain. For this specific problem, the optimalilty criteria based algorithm appears to have terminated in local optima for the DKQ and ANS elements.

	Optimal topology generated using:		
	DKQ	ANS	SRI
Analysed with DKQ	0.0000	2.6995	-4.6636
Analysed with ANS	3.4167	0.0000	-8.5961
Analysed with SRI	16.4448	10.6660	0.0000
Constraint value	-5.2541e-05	2.3863e-05	2.5479e-05

Table B.14: Percentage difference: Corner supported square plate subjected to center point load, single layer model, $t = 0.1$.

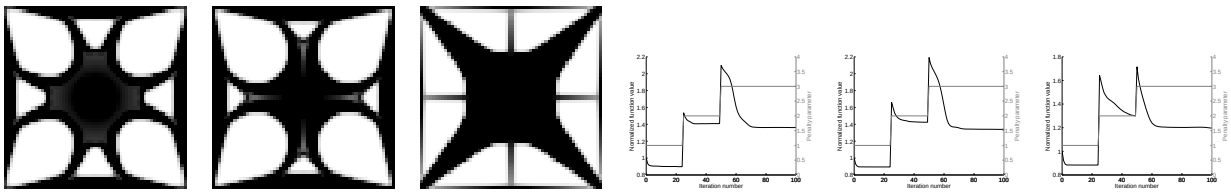

(a) DKQ. (b) ANS. (c) SRI. (d) DKQ. (e) ANS. (f) SRI.

Figure B.15: Optimal topologies of a corner supported square plate subjected to center point load, single layer model, $t = 0.1$: (a)-(c) optimal topologies, (d)-(f) convergence histories.

To confirm this, the same problem was run with identical finite element settings using the well-known MMA algorithm of Svanberg [10]. The optimal topologies for the MMA run are depicted in Figure B.16 with analysis of results in Table B.15. Ironically upon employing MMA as optimizer the results are reversed and the ANS element finds a superior design! Although for this specific problem the optimality criteria based updating scheme is unable to find the globally optimal solution for the ANS or DKQ elements, the effect of the finite element employed on 'optimal topology' is clearly demonstrated. This problem in particular serves also as a demonstration of the complexity (in global optimization terms) of the topology optimization problem.

	Optimal topology generated using:		
	DKQ	ANS	SRI
Analysed with DKQ	0.0000	-4.9705	3.4879
Analysed with ANS	15.2086	0.0000	10.0908
Analysed with SRI	6.5512	-9.4479	0.0000
Constraint value	-2.8216e-03	-9.8052e-04	-1.5108e-03

Table B.15: Percentage difference

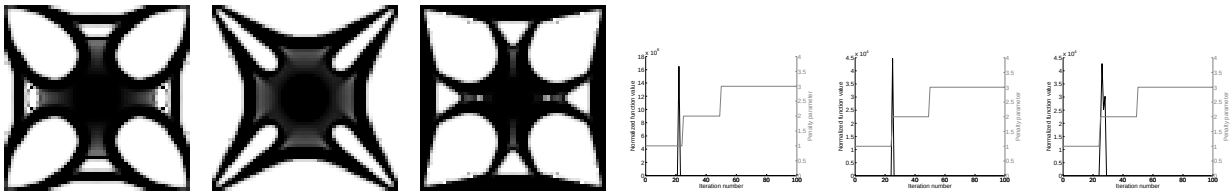

(a) DKQ. (b) ANS. (c) SRI. (d) DKQ. (e) ANS. (f) SRI.

Figure B.16: Optimal topologies of a corner supported square plate subjected to center point load, single layer model, $t = 0.1$: (a)-(c) optimal topologies, (d)-(f) convergence histories. Solved using MMA not OC.

Ribbed material model

Note that the results for the thin ribbed material model are presented and discussed in Section 6.5.3 on page 168. Considering the thick plate results for the ribbed material model, depicted in Figure B.17, again a distinctly different topology results from the use of Mindlin-Reissner elements. The numerical problems encountered with the SRI elements in the thin plate analysis are not experienced in this case. The negative values in the first row of Table B.16 indicate that the thick plate results is marginally superior, even for thin plates.

	Optimal topology generated using:		
	DKQ	ANS	SRI
Analysed with DKQ	0.0000	-0.2379	-0.1029
Analysed with ANS	4.2660	0.0000	0.0515
Analysed with SRI	4.4234	-0.0099	0.0000
Constraint value	-3.3457e-05	-2.8658e-05	-2.1399e-06

Table B.16: Percentage difference: Corner supported square plate subjected to center point load, ribbed model, $t = 0.1$.

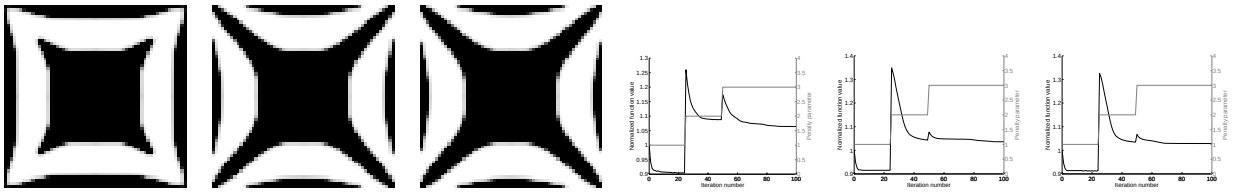

(a) DKQ. (b) ANS. (c) SRI. (d) DKQ. (e) ANS. (f) SRI.

Figure B.17: Optimal topologies of a corner supported square plate subjected to center point load, ribbed model, $t = 0.1$: (a)-(c) optimal topologies, (d)-(f) convergence histories.

Honeycomb material model

The results for the corner supported plate subjected to center point load with the thin honeycomb material model are depicted in Figure B.18. Again, although all converged topologies are similar, the iteration history of the SRI element suggests that some numerical instabilities occurred. In this case, many elements with negative compliance (or positive compliance gradient) were encountered at iteration 90. Figure B.19 illustrates how each of the element used to analyze the thick honeycomb material model, result in different topologies. In this case, the SRI element did not encounter any numerical problems in the iteration history. Although the SRI and ANS topologies (and shapes) are different, the compliance of the two structures is very similar. However, this problem demonstrates that even the two Mindlin-Reissner based elements result in different optimal shapes and topologies even though no numerical problems were encountered during the optimization history.

	Optimal topology generated using:		
	DKQ	ANS	SRI
Analysed with DKQ	0.0000	0.0331	0.0469
Analysed with ANS	0.0046	0.0000	0.0103
Analysed with SRI	0.0184	0.0065	0.0000
Constraint value	-1.5311e-04	3.8396e-05	-2.0403e-04

Table B.17: Percentage difference: Corner supported square plate subjected to center point load, honeycomb model, $t = 0.01$.

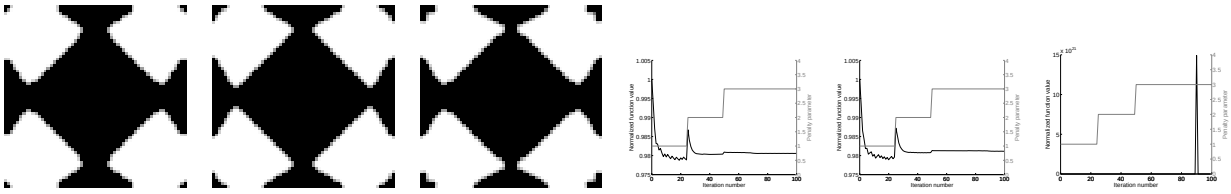

(a) DKQ. (b) ANS. (c) SRI. (d) DKQ. (e) ANS. (f) SRI.

Figure B.18: Optimal topologies of a corner supported square plate subjected to center point load, honeycomb model, $t = 0.01$: (a)-(c) optimal topologies, (d)-(f) convergence histories.

	Optimal topology generated using:		
	DKQ	ANS	SRI
Analysed with DKQ	0.0000	0.3268	0.6250
Analysed with ANS	1.8237	0.0000	0.1043
Analysed with SRI	3.3749	0.0978	0.0000
Constraint value	-1.5311e-04	2.7573e-04	6.2309e-05

Table B.18: Percentage difference: Corner supported square plate subjected to center point load, honeycomb model, $t = 0.1$.

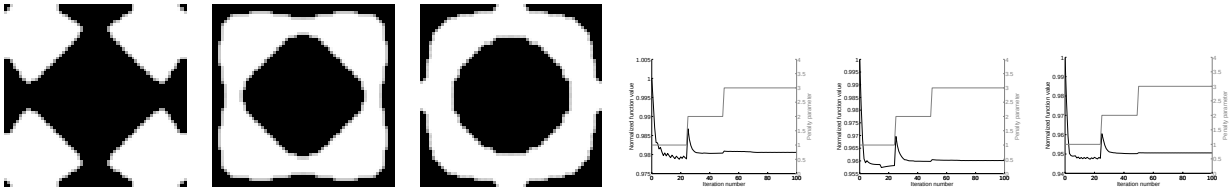

(a) DKQ. (b) ANS. (c) SRI. (d) DKQ. (e) ANS. (f) SRI.

Figure B.19: Optimal topologies of a corner supported square plate subjected to center point load, honeycomb model, $t = 0.1$: (a)-(c) optimal topologies, (d)-(f) convergence histories.

B.2.4 Corner supported square plate with distributed load

In this problem the same corner supported geometry and restraints, depicted in Figure 6.9(c), are used but the applied load in this case is uniformly distributed over the plate surface. In order to ensure that the load is not design dependent, only the ribbed and honeycomb material models are considered. The results for the thin ribbed material model are not repeated here since they are presented in Section 6.5.3, on page 168.

Figure B.20 depicts the optimal topologies for the thick ribbed models, with analysis in Table B.19. The results for the honeycomb material model are shown in Figures B.21 and B.22 with compliance results presented in Tables B.20 and B.21.

Ribbed material model

For the thick plate, again DKQ results in the same topology as the thin plate analysis, while the result of the ANS element is distinctly different. The compliance of the DKQ result is almost 3% higher than that of the ANS result when analysed with ANS plate elements. Again, the SRI element has an extremely irratic convergence history and a completely spurious, unsymmetric optimal topology results.

	Optimal topology generated using:		
	DKQ	ANS	SRI
Analysed with DKQ	0.0000	0.6072	34.2893
Analysed with ANS	2.7370	0.0000	34.5983
Analysed with SRI	121.3774	713.3591	0.0000
Constraint value	3.0994e-05	-3.2532e-05	-3.4844e-05

Table B.19: Percentage difference: Corner supported square plate subjected to uniform distributed load, ribbed model, $t = 0.1$.

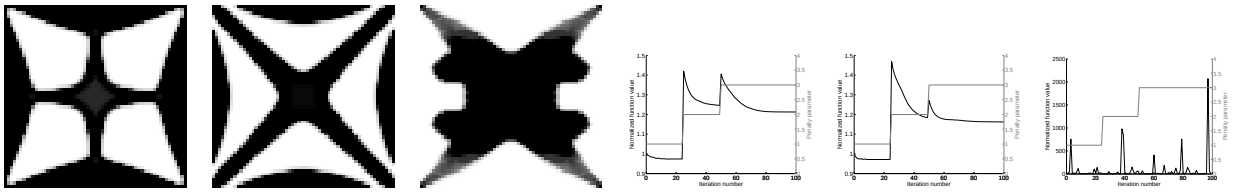

(a) DKQ. (b) ANS. (c) SRI. (d) DKQ. (e) ANS. (f) SRI.

Figure B.20: Optimal topologies of a corner supported square plate subjected to uniform distributed load, ribbed model, $t = 0.1$: (a)-(c) optimal topologies, (d)-(f) convergence histories.

Honeycomb material model

Similar observations can be made for the honeycomb layered models, depicted in Figures B.21 and B.22, with compliance analysis in Tables B.20 and B.21. The displaced shape of the thick honeycomb topologies computed with DKQ and ANS elements respectively, and analyzed using SRI elements, are plotted in Figures B.23 and B.24. In both the thin and thick honeycomb material models (especially the thin model), the compliance of the final topology computed with SRI elements is extremely large, due to the propagating mode. Therefore, the DKQ and ANS optimal topologies appear to be much better in Table B.20 since they are compared to a structure with almost zero stiffness.

	Optimal topology generated using:		
	DKQ	ANS	SRI
Analysed with DKQ	0.0000	0.0031	1.5821
Analysed with ANS	-0.0017	0.0000	1.9462
Analysed with SRI	-99.6858	-99.6666	0.0000
Constraint value	1.9059e-04	1.7756e-04	-8.6728e-03

Table B.20: Percentage difference: Corner supported square plate subjected to uniform distributed load, honeycomb model, $t = 0.01$.

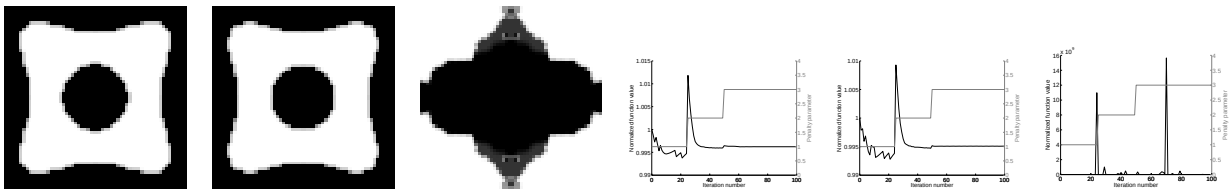

(a) DKQ. (b) ANS. (c) SRI. (d) DKQ. (e) ANS. (f) SRI.

Figure B.21: Optimal topologies of a corner supported square plate subjected to uniform distributed load, honeycomb model, $t = 0.01$: (a)-(c) optimal topologies, (d)-(f) convergence histories.

	Optimal topology generated using:		
	DKQ	ANS	SRI
Analysed with DKQ	0.0000	0.1147	1.5020
Analysed with ANS	0.2618	0.0000	2.1867
Analysed with SRI	2344.5765	-22.7655	0.0000
Constraint value	1.9057e-04	4.6099e-05	7.0618e-04

Table B.21: Percentage difference: Corner supported square plate subjected to uniform distributed load, honeycomb model, $t = 0.1$.

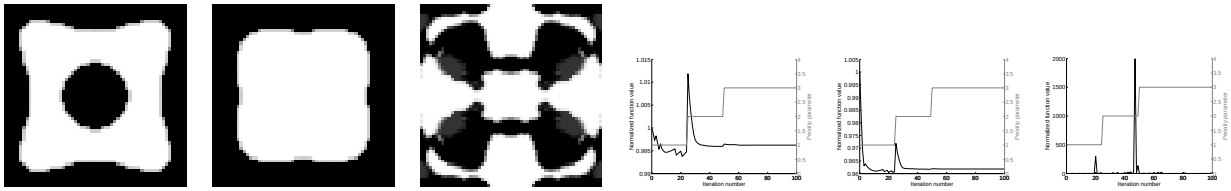

(a) DKQ. (b) ANS. (c) SRI. (d) DKQ. (e) ANS. (f) SRI.

Figure B.22: Optimal topologies of a corner supported square plate subjected to uniform distributed load, honeycomb model, $t = 0.1$: (a)-(c) optimal topologies, (d)-(f) convergence histories.

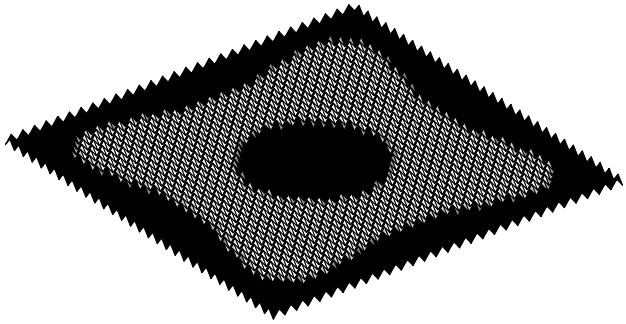

Figure B.23: Optimal topology, computed using DKQ, of the corner supported plate subjected to distributed load with thick honeycomb material model: Displaced shape analyzed using SRI elements, amplification factor 1×10^{-4}.

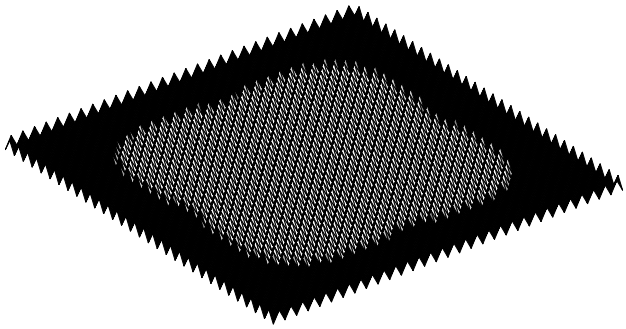

Figure B.24: Optimal topology, computed using ANS, of the corner supported plate subjected to distributed load with thick honeycomb material model: Displaced shape analyzed using SRI elements, amplification factor 1×10^{-4}.

B.3 Additional shell results

In the final section of this appendix, results not included in Section 6.5.5 are offered.

B.3.1 Cylindrical shell

The first shell problem is depicted in Figure 6.15. The geometry, restraints, applied loads and material properties are all depicted in the figure. The symmetry of the problem is exploited by only modeling one quarter of the structure with a 30×30 discretization. Once again, results are reported for the single layer, ribbed and honeycomb material models. A volume constraint of half of the design volume is again imposed.

Single layer material model

Figures B.25 and B.26 present details of the optimal topologies depicted in Figure 6.16, and their corresponding convergence histories. Since the x-axis of Figure 6.16 is plotted on a logarithmic scale, the topology at $\alpha = 0$ could not be included.

Figures B.25(a) and B.25(g) depict the optimal topologies for $\alpha = 0$ using the Q4αDKQ and Q4γDKQ elements respectively, with convergence histories in Figures B.26(a) and B.26(g), respectively. Notably, the Q4αDKQ has numerical instabilities if no stiffness is allotted to the rotational DOFs. No such problem is encountered when employing the Q4γDKQ element. The stability of the Q4γDKQ element at $\alpha = 0$ is due to the fact that α (which only scales γ) eliminates the penalty matrix $\boldsymbol{p}_{\mathrm{m}}^{\gamma} = \mathbf{0}$ in (6.29). However, enough stiffness is present to prevent numerical problems in the topology optimization environment. Of course this does not mean that the value of compliance will be very accurately calculated, and since this element is rank deficient its use in general should be avoided.

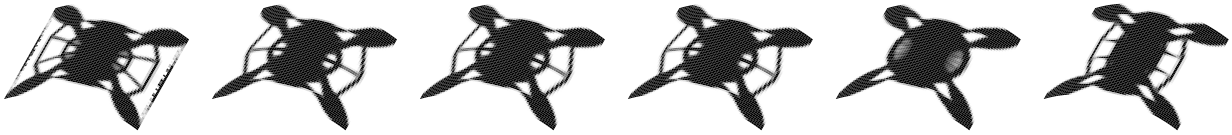

(a) Q4αDKQ element, $\alpha = 0$.

(b) Q4αDKQ element, $\alpha = 10^{-6}$.

(c) Q4αDKQ element, $\alpha = 10^{-4}$.

(d) Q4αDKQ element, $\alpha = 10^{-2}$.

(e) Q4αDKQ element, $\alpha = 10^{0}$.

(f) Q4αDKQ element, $\alpha = 10^{2}$.

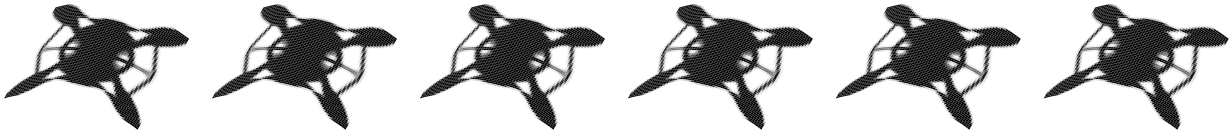

(g) Q4γDKQ element, $\alpha = 0$.

(h) Q4γDKQ element, $\alpha = 10^{-6}$.

(i) Q4γDKQ element, $\alpha = 10^{-4}$.

(j) Q4γDKQ element, $\alpha = 10^{-2}$.

(k) Q4γDKQ element, $\alpha = 10^{0}$.

(l) Q4γDKQ element, $\alpha = 10^{2}$.

Figure B.25: Optimal topologies of corner supported cylinder with single layer material model for various values of α.

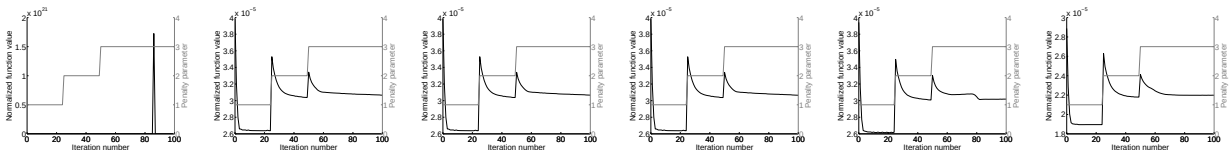

(a) Q4αDKQ element, $\alpha = 0$.

(b) Q4αDKQ element, $\alpha = 10^{-6}$.

(c) Q4αDKQ element, $\alpha = 10^{-4}$.

(d) Q4αDKQ element, $\alpha = 10^{-2}$.

(e) Q4αDKQ element, $\alpha = 10^{0}$.

(f) Q4αDKQ element, $\alpha = 10^{2}$.

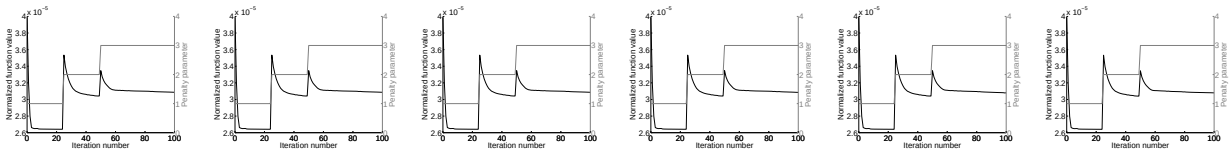

(g) Q4γDKQ element, $\alpha = 0$.

(h) Q4γDKQ element, $\alpha = 10^{-6}$.

(i) Q4γDKQ element, $\alpha = 10^{-4}$.

(j) Q4γDKQ element, $\alpha = 10^{-2}$.

(k) Q4γDKQ element, $\alpha = 10^{0}$.

(l) Q4γDKQ element, $\alpha = 10^{2}$.

Figure B.26: Convergence histories for corner supported cylinder with single layer material model for various values of α.

Ribbed material model

Figure B.27 depicts the optimal topologies, as well as the function and constraint values, for the ribbed material model as a function of scaling parameter α. Again, the results for the Q4αDKQ element differ from the Q4γDKQ results at high values of α. Conversely, the optimal topologies calculated using the Q4γDKQ element are relatively insensitive to α.

Figures B.29(a) once again indicate that, with α is set to zero, an unstable convergence history results for the Q4αDKQ element is recorded, although the a 'correct' optimal topology results. Figure B.29(g) confirms that no such problems are encountered when employing the Q4γDKQ element.

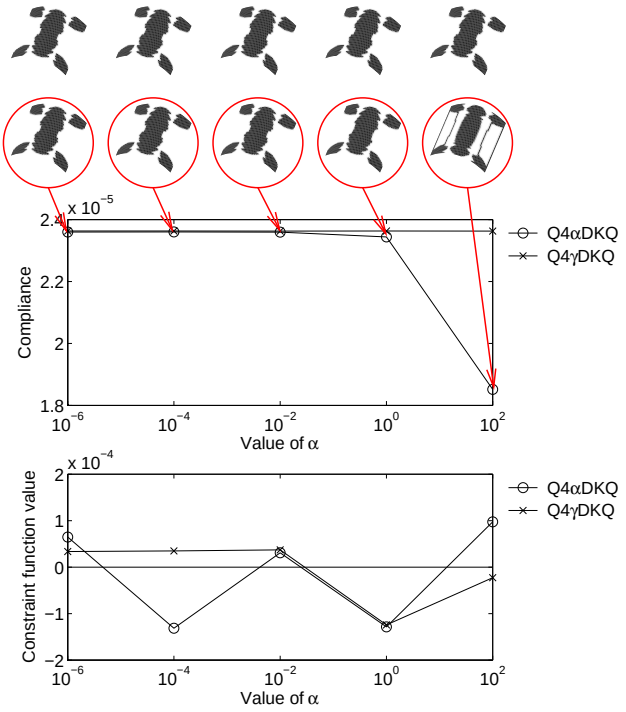

Figure B.27: Optimal topologies of a corner supported cylinder with ribbed material model. Above are the optimal topologies solved employing the standard Q4γDKQ element. On the second row are the optimal topologies employing Q4αDKQ for various values of scaling factor α. Also shown are the optimal function and constraint values for various values of scaling factor α.

(a) Q4αDKQ element, $\alpha = 0$.

(b) Q4αDKQ element, $\alpha = 10^{-6}$.

(c) Q4αDKQ element, $\alpha = 10^{-4}$.

(d) Q4αDKQ element, $\alpha = 10^{-2}$.

(e) Q4αDKQ element, $\alpha = 10^{0}$.

(f) Q4αDKQ element, $\alpha = 10^{2}$.

(g) Q4γDKQ element, $\alpha = 0$.

(h) Q4γDKQ element, $\alpha = 10^{-6}$.

(i) Q4γDKQ element, $\alpha = 10^{-4}$.

(j) Q4γDKQ element, $\alpha = 10^{-2}$.

(k) Q4γDKQ element, $\alpha = 10^{0}$.

(l) Q4γDKQ element, $\alpha = 10^{2}$.

Figure B.28: Optimal topologies of corner supported cylinder with ribbed material model for various values of α.

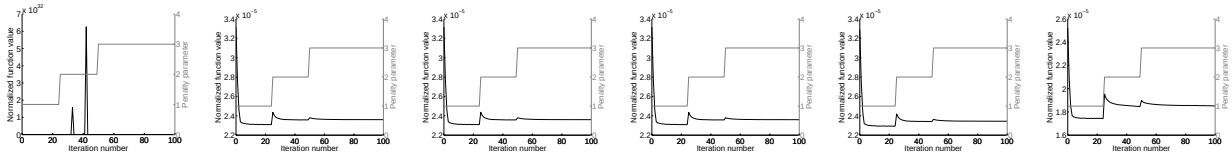

(a) Q4αDKQ element, $\alpha = 0$.

(b) Q4αDKQ element, $\alpha = 10^{-6}$.

(c) Q4αDKQ element, $\alpha = 10^{-4}$.

(d) Q4αDKQ element, $\alpha = 10^{-2}$.

(e) Q4αDKQ element, $\alpha = 10^{0}$.

(f) Q4αDKQ element, $\alpha = 10^{2}$.

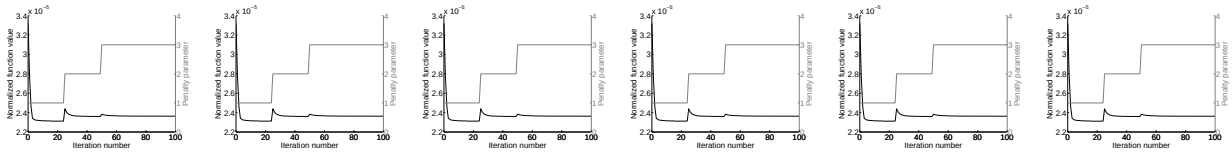

(g) Q4γDKQ element, $\alpha = 0$.

(h) Q4γDKQ element, $\alpha = 10^{-6}$.

(i) Q4γDKQ element, $\alpha = 10^{-4}$.

(j) Q4γDKQ element, $\alpha = 10^{-2}$.

(k) Q4γDKQ element, $\alpha = 10^{0}$.

(l) Q4γDKQ element, $\alpha = 10^{2}$.

Figure B.29: Convergence histories for corner supported cylinder with ribbed material model for various values of α.

Honeycomb material model

Finally, the optimal topologies for the honeycomb material model, are presented in Figure B.30. Again, the sensitivity of optimal topologies using Q4αDKQ elements is highlighted, in contrast to the Q4γDKQ element. Figure B.32(a) shows that although the optimal topology of the Q4αDKQ element corresponds to that using Q4γDKQ elements, some numerical instabilities are once again encountered when $\alpha = 0$ in the Q4αDKQ element.

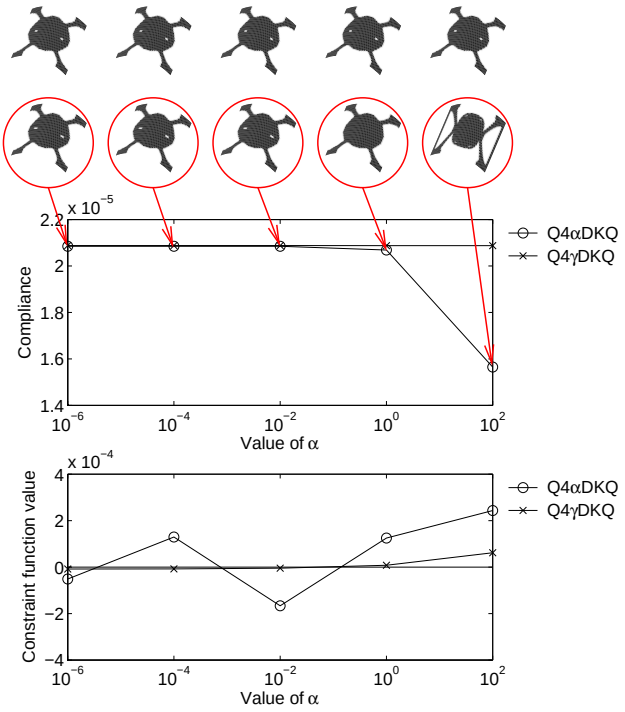

Figure B.30: Optimal topologies of a corner supported cylinder with honeycomb material model. Above are the optimal topologies solved employing the standard Q4γDKQ element. On the second row are the optimal topologies employing Q4αDKQ for various values of scaling factor α. Also shown are the optimal function and constraint values for various values of scaling factor α.

B.3.2 Pretwisted beam

The final shell example is depicted in Figure 6.17. The problem is that of a pretwisted beam, which is clamped at the root, with two point loads applied at the vertices opposite the fixed end. The full geometry is modeled with a 40×40 discretization. A volume constraint of half of the design volume is imposed. For brevity, only the single layer results will be presented. This problem has previously been shown to be sensitive to the value of α [135].

For this problem, the range of values of α for which the Q4αDKQ and Q4γDKQ elements result in similar topologies is much smaller than the cylindrical shell problem. In fact, Figure B.33 shows that values of $\alpha = 0,\ 10^{-6},\ 10^{-4}$ and 10^{-2}, each result in different topologies when

the finite element model employs Q4αDKQ elements! In contrast, the Q4γDKQ element is once again shown to be stable for all tested values of α.

Single layer material model

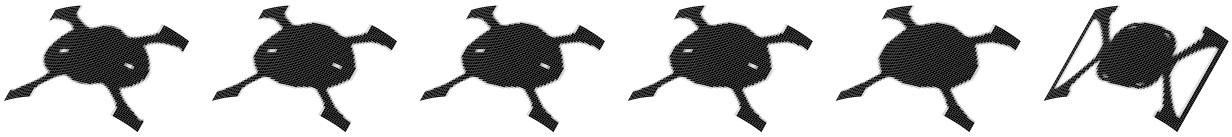

(a) Q4αDKQ element, $\alpha = 0$.

(b) Q4αDKQ element, $\alpha = 10^{-6}$.

(c) Q4αDKQ element, $\alpha = 10^{-4}$.

(d) Q4αDKQ element, $\alpha = 10^{-2}$.

(e) Q4αDKQ element, $\alpha = 10^{0}$.

(f) Q4αDKQ element, $\alpha = 10^{2}$.

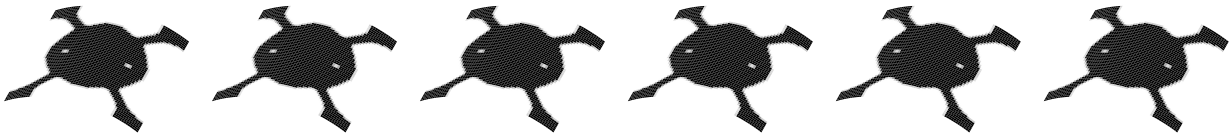

(g) Q4γDKQ element, $\alpha = 0$.

(h) Q4γDKQ element, $\alpha = 10^{-6}$.

(i) Q4γDKQ element, $\alpha = 10^{-4}$.

(j) Q4γDKQ element, $\alpha = 10^{-2}$.

(k) Q4γDKQ element, $\alpha = 10^{0}$.

(l) Q4γDKQ element, $\alpha = 10^{2}$.

Figure B.31: Optimal topologies of corner supported cylinder with honeycomb material model for various values of α.

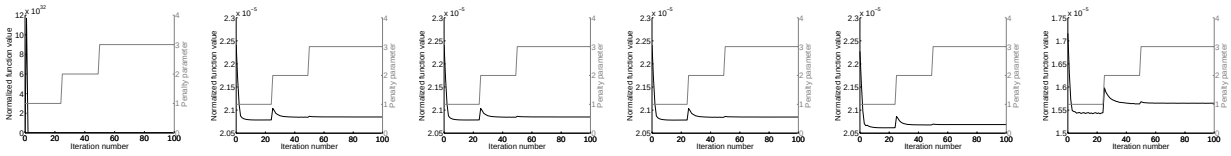

(a) Q4αDKQ element, $\alpha = 0$.

(b) Q4αDKQ element, $\alpha = 10^{-6}$.

(c) Q4αDKQ element, $\alpha = 10^{-4}$.

(d) Q4αDKQ element, $\alpha = 10^{-2}$.

(e) Q4αDKQ element, $\alpha = 10^{0}$.

(f) Q4αDKQ element, $\alpha = 10^{2}$.

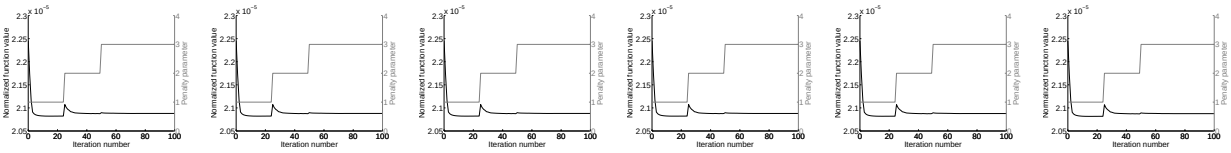

(g) Q4γDKQ element, $\alpha = 0$.

(h) Q4γDKQ element, $\alpha = 10^{-6}$.

(i) Q4γDKQ element, $\alpha = 10^{-4}$.

(j) Q4γDKQ element, $\alpha = 10^{-2}$.

(k) Q4γDKQ element, $\alpha = 10^{0}$.

(l) Q4γDKQ element, $\alpha = 10^{2}$.

Figure B.32: Convergence histories for corner supported cylinder with honeycomb material model for various values of α.

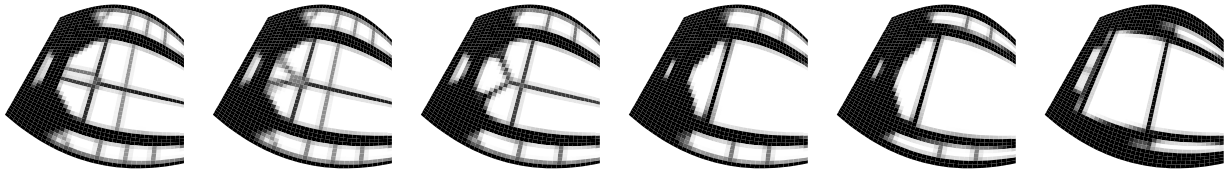

(a) Q4αDKQ element, $\alpha = 0$.

(b) Q4αDKQ element, $\alpha = 10^{-6}$.

(c) Q4αDKQ element, $\alpha = 10^{-4}$.

(d) Q4αDKQ element, $\alpha = 10^{-2}$.

(e) Q4αDKQ element, $\alpha = 10^{0}$.

(f) Q4αDKQ element, $\alpha = 10^{2}$.

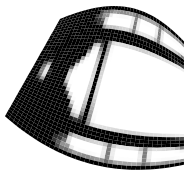

(g) Q4γDKQ element, $\alpha = 0$.

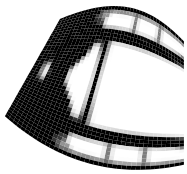

(h) Q4γDKQ element, $\alpha = 10^{-6}$.

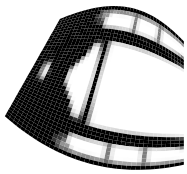

(i) Q4γDKQ element, $\alpha = 10^{-4}$.

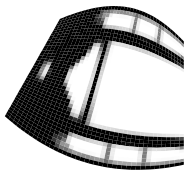

(j) Q4γDKQ element, $\alpha = 10^{-2}$.

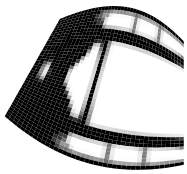

(k) Q4γDKQ element, $\alpha = 10^{0}$.

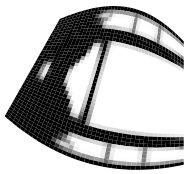

(l) Q4γDKQ element, $\alpha = 10^{2}$.

Figure B.33: Optimal topologies of pretwisted beam with single layer material model for various values of α.

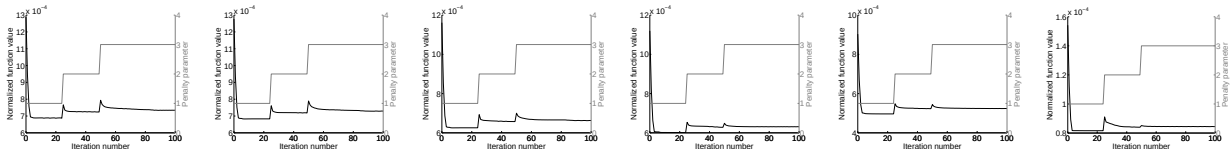

(a) Q4αDKQ element, $\alpha = 0$.

(b) Q4αDKQ element, $\alpha = 10^{-6}$.

(c) Q4αDKQ element, $\alpha = 10^{-4}$.

(d) Q4αDKQ element, $\alpha = 10^{-2}$.

(e) Q4αDKQ element, $\alpha = 10^{0}$.

(f) Q4αDKQ element, $\alpha = 10^{2}$.

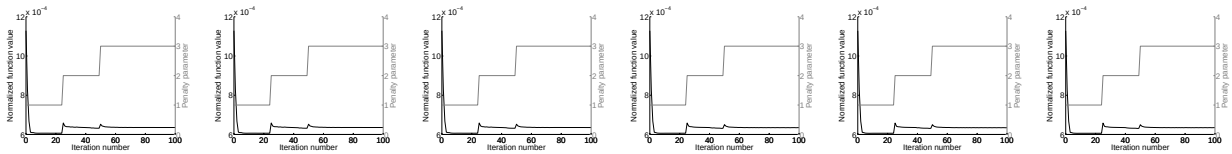

(g) Q4γDKQ element, $\alpha = 0$.

(h) Q4γDKQ element, $\alpha = 10^{-6}$.

(i) Q4γDKQ element, $\alpha = 10^{-4}$.

(j) Q4γDKQ element, $\alpha = 10^{-2}$.

(k) Q4γDKQ element, $\alpha = 10^{0}$.

(l) Q4γDKQ element, $\alpha = 10^{2}$.

Figure B.34: Convergence histories for pretwisted beam with single layer material model for various values of α.